NASA Public Access
Author manuscript
Q J R Meteorol Soc. Author manuscript; available in PMC 2019 November 01.

Published in final edited form as:
Q J R Meteorol Soc. 2018 November ; 144(51): 27–48. doi:10.1002/qj.3313.

The Global Precipitation Measurement (GPM) mission's scientific achievements and societal contributions: reviewing four years of advanced rain and snow observations

Gail Skofronick-Jackson[1], **Dalia Kirschbaum**[1], **Walter Petersen**[2], **George Huffman**[1], **Chris Kidd**[3,1], **Erich Stocker**[1], and **Ramesh Kakar**[4]

[1]Code 612.0, NASA Goddard Space Flight Center, Greenbelt, MD

[2]ST11, NASA Marshall Space Flight Center, Earth Sciences Office, National Space and Technology Center, Huntsville, AL

[3]Earth System Science Interdisciplinary Center, University of Maryland, College Park, MD

[4]NASA Headquarters, Washington, D.C

Abstract

Precipitation represents a life-critical energy and hydrologic exchange between the Earth's atmosphere and its surface. As such, knowledge of where, when, and how much rain and snow falls is essential for scientific research and societal applications. Building on the 17-year success of the Tropical Rainfall Measurement Mission (TRMM), the Global Precipitation Measurement (GPM) Core Observatory (GPM-CO) is the first U.S. National Aeronautical and Space Administration (NASA) satellite mission specifically designed with sensors to observe the structure and intensities of both rain and falling snow. The GPM-CO has proved to be a worthy successor to TRMM, extending and improving high-quality active and passive microwave observations across all times of day. The GPM-CO launched in early 2014, is a joint mission between NASA and the Japanese Aerospace Exploration Agency (JAXA), with sensors that include the NASA-provided GPM Microwave Imager and the JAXA-provided Dual-frequency Precipitation Radar. These sensors were devised with high accuracy standards enabling them to be used as a reference for inter-calibrating a constellation of partner satellite data. These intercalibrated partner satellite retrievals are used with infrared data to produce merged precipitation estimates at temporal scales of 30 minutes and spatial scales of 0.1° × 0.1°. Precipitation estimates from the GPM-CO and partner constellation satellites, provided in near real time and later reprocessed with all ancillary data, are an indispensable source of precipitation data for operational and scientific users. Advances have been made using GPM data, primarily in improving sensor calibration, retrieval algorithms, and ground validation measurements, and used to further our understanding of the characteristics of liquid and frozen precipitation and the science of water and hydrological cycles for climate/weather forecasting. These advances have extended to societal benefits related to water resources, operational numerical weather prediction, hurricane monitoring, prediction, and disaster response, extremes, and disease.

NASA Author Manuscript
NASA Author Manuscript
NASA Author Manuscript

NASA Author Manuscript NASA Author Manuscript NASA Author Manuscript

Keywords

precipitation; satellite; rain; snow; remote sensing; applications

1. Introduction

The 21st century poses substantial challenges for the sustainable management of the Earth's water resources at all levels from the local to the global scale. The international climate community through the World Climate Research Programme (WCRP) identified seven grand challenges facing both our understanding of, and our ability to adapt to climate change (http://wcrp-climate.org/grand-challenges). Four of these challenges relate to atmospheric water: Clouds, Circulation, and Climate Sensitivity; Weather and Climate Extremes; Water for the Food Baskets of the World; and Near-Term Climate Prediction. Three basic questions posed under these challenges are: How will the availability of fresh water change in the coming decades, what is the predictability of changes in the frequency and intensity of extremes at seasonal to decadal time scales, and how does convection shape cloud feedbacks? Central to these questions is the need for better measurements of precipitation, from observing global patterns, to local scales where it has the most profound societal impact, and to microphysical scales to study the characteristics of rain and snow hydrometeors.

The Global Precipitation Measurement (GPM) mission is a scientific undertaking to understand the physics and space-time variability of the Earth's global precipitation as a key component of its weather, climate, and hydrological systems. In 2014, NASA and the Japan Aerospace Exploration Agency (JAXA) launched the GPM Core Observatory (GPM-CO) spacecraft. The GPM-CO carries the most advanced precipitation sensors currently in space. These sensors include the Ku and Ka-band Dual-frequency Precipitation Radar (DPR) provided by JAXA that measures three-dimensional (3D) structures of precipitation, and the GPM Microwave Imager (GMI), a well-calibrated multi-frequency radiometer capable of providing wide-swath precipitation data. The capability and swath characteristics of the GPM-CO are illustrated in Figure 1. This figure depicts the retrievals from the DPR and GMI for an overpass of a storm on 17 December 2016 with falling snow (in blues) detected and estimated over land and a thin convective line of rain (in green and red) just off the coast of North and South Carolina. The GPM-CO was designed to measure rain rates from 0.2–110.0 mm h^{-1}, to detect moderate to intense snow events, and to serve as a precipitation physics laboratory. The GPM-CO, a key part of the GPM mission (Skofronick-Jackson *et al.*, 2017), is designed to be the calibration reference standard for unifying the data from a constellation of approximately 10 partner satellites as listed in Hou *et al.* (2014). Table I provides information on the constellation members, sensors, types and launches. This constellation provides the observations for the GPM mission's next-generation, merged global precipitation estimates at high temporal and spatial resolutions. The products from the Integrated Multi-satellitE Retrievals for GPM (IMERG), NASA's uniformly gridded precipitation product, are one of GPM's most popular data products.

NASA Author Manuscript NASA Author Manuscript NASA Author Manuscript

The four years of GPM-CO data to date, along with the 17 years of data from GPM's predecessor, the Tropical Rainfall Measuring Mission (TRMM; Kummerow *et al.*, 2000), have generated, and will continue to contribute to, accurate records of global, regional, convective, and microphysical precipitation patterns. The inter-calibration of the TRMM Microwave Imager (TMI) and pre-GPM microwave constellation sensor data to GMI's highly accurate data is expected to be released in 2018, along with inter-calibrated TRMM Precipitation Radar (PR) and DPR data. As a result, GPM will generate a consistent, uniform, and long-term precipitation record[1] that covers both the TRMM and GPM eras, potentially stretching over 30 years subject to the GPM-CO fuel, instruments, and operations.

The observations from GPM and TRMM can be used for characterizing changes in the Earth's water cycle, quantifying freshwater fluxes and reservoirs, and advancing our predictive capability of natural hazards and extreme weather events. There are far-reaching impacts for the Earth system (Trenberth, 2011; Intergovernmental Panel on Climate Change (IPCC), 2014) from precipitation falling on and interacting with the land surface (landslides, floods, erosion, etc.), the ocean surface (salinity, sea surface temperature, density, etc.), and sea ice/glaciers (growth or decay depending on rain or snow amounts). TRMM-based research has already investigated changes in the global Earth system in terms of precipitation (e.g., climatology: Wang *et al.*, 2014; distribution: Liu and Zipser, 2009; El Nino Southern Oscillation (ENSO): Arndt *et al.*, 2010; Madden-Julian Oscillation (MJO): Lau and Wu, 2010). The higher frequency channels on DPR (Ka) and GMI (166 and 183 GHz) were specifically added to the GPM-CO's design to be sensitive to frozen hydrometeors both above the melting layer, where frozen precipitation is responsible for 50% of global rainfall (Field and Heymsfield, 2015), and snow falling at the Earth's surface.

Precipitation information must be used synergistically with complementary observations to gain physical insights into the complex interactions between water and other components of the Earth system (e.g., Kucera *et al.*, 2013; Liu and Xie, 2017). Research has demonstrated the value of precipitation data for improving the outputs of weather prediction models (e.g., Geer *et al.*, 2017; Kim *et al.*, 2017; Chambon *et al.*, 2014). Precipitation data are critical to the assessment of global climate models and reanalysis systems, for example, Kidd *et al.* (2013) evaluated the ability of operational numerical models and satellite estimates to properly represent the diurnal cycle of precipitation, while Kim and Alexander (2013) compared TRMM estimates to five reanalysis models to investigate the variability in convectively coupled equatorial waves at submonthly time scales.

The GPM ground validation (GV) program, through its connection to atmospheric and surface modelling and observations, plays a key role in combining observations from diverse sources into a coherent framework. Direct statistical, physical, and hydrologic validation have been fundamental in verifying and improving GPM algorithms for the DPR, GMI, and combined GMI+DPR products. Field campaigns conducted by the GPM mission and its

[1]Such long records take two forms, the Climate Data Record (CDR), which emphasizes climate-scale homogeneity, and the High Resolution Precipitation Product (HRPP), which provides the "best" snapshot estimates (Tapiador *et al.*, 2017). The individual TRMM and GPM precipitation records approximate CDRs, while IMERG is best characterized as a HRPP.

NASA Author Manuscript NASA Author Manuscript NASA Author Manuscript

partners have explored a wide range of precipitation processes across numerous environmental settings. In the past seven years, GPM-sponsored field campaigns (see Figure 2) have observed high latitude light rain and snow in Finland (LPVEX), mid-latitude convective rain over the United States (MC3E), falling snow and cold season processes in Canada (GCPEX), heavy rainfall and flooding in Iowa (IFloodS), mid-latitude continental orographic processes and hydrometeorological impacts/modelling (IPHEX), and mid-latitude coastal/continental mixed-phase, land/ocean and complex terrain processes (OLYMPEX).

From the start, GPM has been designed to be a mission with both scientific and societal goals. The GPM suite of products contributes to a wide range of societal applications, many initially developed with TRMM data, such as: tropical and extratropical cyclone tracking and rainfall monitoring, famine early warning, drought monitoring, water resource management, agricultural forecasting, numerical weather prediction, land surface modelling, global climate modelling, disease monitoring, economic studies, and animal migration. Many of these applications require near-real-time (NRT) data as well as longer-term, well-calibrated merged-satellite precipitation information (e.g., Reed *et al.*, 2015); the GPM mission provides both of these product latencies. The U.S. GPM team's IMERG product (Huffman *et al.* 2017) is being used as an input for hazard assessment and forecasting for floods, landslides, fires, agriculture yield prediction, famine onset, and disease outbreaks (e.g., Wu *et al.*, 2014; Kirshbaum *et al.*, 2015a,b; Field *et al.*, 2015), particularly in regions where adequate ground-based information is lacking. Selected applications are also reported in Kirschbaum *et al.* (2017), and Kucera *et al.* (2013). GPM data are also valuable for communities assessing the environmental impacts of climate change (National Research Council, 2013), and disasters. Figure 3 shows a one-week accumulation of precipitation from 16–22 July 2017, from the IMERG product. The image shows important precipitation features such as the Intertropical Convergence Zone (ITCZ) located along 10°N latitude across the eastern Pacific and Atlantic, and the Asian summer monsoon over the Indian sub-continent and southeast Asia, along with long streaks of precipitation associated with Hurricane Fernanda in the eastern Pacific between 10°−20°N and 140°−110°W.

Since launch, the GPM-CO instruments, spacecraft, ground systems, and data processing systems have all been operating at peak performance. Notable achievements in the first three years of operations include updated algorithms incorporating the improved calibration of the DPR, use of the dual-frequency DPR data to construct global databases of the drop size distribution (DSD) for use in single frequency radar rain retrievals, an observational database for the GMI retrieval algorithm, and improved representation of light rain, falling snow, and non-spherical particles. Scientifically, the GPM mission has been able to: provide a better understanding of falling snow microphysics with results showing that consideration of non-spherical particles in retrieval databases are essential (Olson *et al.,* 2016); use the GPM-CO data as a reliable transfer standard for the constellation partner precipitation sensors to ensure calibrated estimates of rain and falling snow; classify the locations of the largest, deepest, and strongest precipitation systems on Earth; and provide additional benefits to weather forecasts, among many applications. This paper highlights some of the technical and scientific achievements of the GPM mission to date and describes how these data have contributed to advancing societal applications. In Section 2 we describe GPM data products.

NASA Author Manuscript NASA Author Manuscript NASA Author Manuscript

Section 3 provides an overview of GPM scientific achievements with respect to the core mission science objectives, while Section 4 describes the ground validation activities. In Section 5 we describe how these data products are being used by the community to enhance a range of societal applications. Finally, conclusions are provided in section 6, together with future perspectives of the GPM mission.

2. Summary of GPM data products

The GPM mission has both NRT and research-quality production requirements for the products listed in Table II. The NRT data are produced using GPM data enhanced with model data or other forms of ancillary data. NRT products include the GMI brightness temperatures (Tb; Draper *et al.*, 2015a) and precipitation retrievals from the GMI and GPM constellation (using the Goddard Profiling Algorithm, GPROF; Kummerow *et al.*, 2015), DPR (Masaki *et al.*, 2015; Seto and Iguchi, 2015), and GPM Combined Radar–Radiometer Algorithm (CORRA; Grecu *et al.*, 2016). The GPM mission requires GMI products to be available within one hour of data collection while both the DPR and CORRA are to be available within 3 hours of data collection, 90% of the time; however, in practice the data are available on average much sooner (Table III). An important NRT national product developed by the NASA team is IMERG, a gridded product that uses both GPM-CO and partner satellite precipitation estimates along with geostationary infrared precipitation estimates to fill in gaps between the microwave satellite overpasses by Lagrangian time interpolation, or "morphing", and monthly gauge information (Huffman *et al.*, 2017). As summarized in Section 3.1, the CORRA product calibrates the partner satellite estimates, while the IR estimates are calibrated by the passive microwave estimates. The IMERG product is available every 30 minutes at a spatial resolution of 0.1°×0.1° (or about 10 km × 10 km at the Equator). JAXA produces an analogous national product called Global Satellite Mapping of Precipitation (GSMaP; Aonashi *et al.*, 2009) that depends on the inter-calibrated brightness temperature products from the GPM constellation computed by the Precipitation Processing System (PPS). All of the NRT products are also processed as research products with delays of hours to months after the observation, when all the required high-quality ancillary and geolocation data are received. The goal of the research products is accuracy, completeness, consistency, and stability for long-term precipitation investigations. In the case of IMERG, the computation is done three times to serve different communities. The Early Run is computed without backward morphing and just using climatological gauge information so that it can be computed within about 4 hours as input to fast-response situations, such as flooding. The Late Run has backward morphing, but still only climatological gauge information, allowing it to be computed about 12 hours after observations as input to next-day kinds of applications, such as crop forecasting and drought analysis. The Final Run includes monthly gauge analyses (from Global Precipitation Climatology Centre) and uses satellite retrievals that make use of high-quality reanalyses. Its latency is about 3 months and is considered the product of choice for research.

GPM data meet mission success requirement metrics (Skofronick-Jackson, 2017). Focusing first on rainfall, Figure 4 demonstrates that the DPR, and CORRA quantify rain rates between 0.2 and 110 mm h^{-1}, while GMI estimates rain rates up to 60 mm h^{-1} due to the averaging of strong convective cells by the coarser resolution radiometer observations. Note

NASA Author Manuscript NASA Author Manuscript NASA Author Manuscript

that at the DPR (GMI) 5-km (15-km) footprint scales, rain rates ≥ 110 mm h^{-1} (60 mm h^{-1}) are very infrequent, and make up less than 0.1% of the rain occurrences over the 2.5-year sample shown. Fig. 4 (right) demonstrates that GPM-CO's instantaneous rain rate bias and uncertainty are excellent, being less than 50% at 1 mm h^{-1} and less than 25 % at 10 mm h^{-1}. The errors are less at 10 mm h^{-1} since this is where both the Ku and Ka channels on DPR are sensitive to the rain and provide additional constraints for both the DPR and CORRA algorithms. In Fig. 4e, the GMI biases run a little high at 1 mm h^{-1}, probably due to the GMI mistaking some land surface features for low rain rates.

While GPM-CO is specifically designed to also observe falling snow, the requirements were only to detect falling snow. Since GPM-CO is exceeding the detection requirements by providing estimates of falling snow in the DPR, CORRA, and GMI products (See Fig. 1), it is essential to begin validating estimates of falling snow. Satellite algorithms for estimating falling snow have yet to reach the level of maturity of the rainfall algorithms, and errors of 100–200% are not unexpected. While surface observations are the natural starting point for validating satellite-based estimates of falling snow, these are fraught with uncertainties (e.g., Rasmussen *et al.,* 2012) and are plagued with the lack of station data (Kidd *et al.*, 2017a). The National Oceanic and Atmospheric Administration (NOAA) Multi-Radar Multi-Sensor (MRMS) data product (see Section 4) based on surface radars provides good estimates of liquid precipitation but the "quality" flag for data usage drops considerably when the precipitation is frozen or mixed-phase, not least because the reflectivity-snow rate (Z-S) relationship is much more variable than the reflectivity-rain rate relationship.

CloudSat (Stephens *et al.,* 2002) is also capable of detecting and estimating falling snow. The CloudSat Cloud Profiling Radar (CPR) has a minimum detectable reflectivity of approximately - 29 dBZ, with falling snow (as opposed to non-precipitating ice particles) detectable to around 15 dBZ. In comparison, the GPM DPR has a minimum detectable reflectivity of around 12–13 dBZ. In order to start assessing the impacts of minimum detectable reflectivity differences between CloudSat and DPR, Figure 5 presents global difference maps (CloudSat – DPR) for various cutoff thresholds of CloudSat radar reflectivity. Figure 5a demonstrates that CloudSat at a −15 dBZ cutoff observes light snowfall that accumulates in the Antarctic and near Greenland and, at a cutoff of 5dBZ (Fig. 5b), CloudSat is still accumulating more snow than the DPR. CloudSat and DPR estimates become similar with CloudSat threshold cutoffs of between 8 and 12 dBZ. The sensitivity differences between CloudSat, which operates at W-band, and DPR, which operates at Ku- and Ka-bands, and the different Z-S relationships used in the two algorithms lead us to anticipate that a zero difference map might not be achievable. Figure 5 indicates that validating snow estimates will not be easy or straightforward from surface-based or satellite based estimates. Nevertheless, such comparison efforts are ongoing as shown in Tang *et al.* (2017), von Lerber *et al.* (2017). Indeed, despite the relatively high sensitivity of the DPR with a minimum detectable rate of 0.2 mmh^{-1}, the DPR has been shown to miss more than 50% of the global snowfall mass estimated by CloudSat (Casella et al., 2017). Concurrent work to improve falling snow retrieval algorithms is underway.

An additional key component in GPM is the PPS system, which captures mission operation downlinked data and archives the GPM-CO and partner brightness temperature files, the

NASA Author Manuscript NASA Author Manuscript NASA Author Manuscript

NOAA/Climate Prediction Center geo-infrared brightness temperature analyses, and ancillary data. Once PPS has acquired the requisite data, it is responsible for computing precipitation estimate products (Table II) from this data, feeding these retrievals into IMERG, hosting the resulting output files, and providing a range of user support, including value-added products. All GPM data are freely available at PPS (https://pmm.nasa.gov/data-access/downloads/gpm) while JAXA's GPM products can be obtained from https://www.gportal.jaxa.jp/gp/top.html or http://sharaku.eorc.jaxa.jp/.

3. Observational goals for GPM precipitation: microphysical to global scales

The five science goals of GPM's data products include: (1) advancing precipitation observations from space; (2) improving knowledge of precipitation systems, water cycle variability, and freshwater availability; and improving (3) hydrological, (4) climate, and (5) weather modelling and prediction. By making precipitation data available in NRT to operational agencies and users beyond the traditional science community, GPM facilitates the use of space-based precipitation observations in a wide range of practical applications to directly benefit society. With these goals in mind, GPM science encompasses not only scientific discovery but also application-oriented research and development.

3.1 Progress toward Advancing Precipitation Measurements

The GPM-CO was specifically designed with highly calibrated instruments and enhanced measurement capabilities for advancing precipitation measurements from space. These GPM-CO observations aim to improve our knowledge of the microphysical properties and vertical structure information of precipitating systems, while the combination of active and passive observations provides a calibration standard for unifying and improving the global precipitation measurements from a constellation of sensors. Assessments of GPM-CO products show that it has accurate rainfall retrievals (Petersen *et al.*, 2016) with sensitivity down to 0.2 mm h^{-1} (e.g., Fig. 5 and Hamada and Takayabu, 2016), has been able to detect falling snow (e.g., You *et al.*, 2016; Munchak and Skofronick-Jackson, 2012; Skofronick-Jackson *et al.*, 2013), and reduced the errors associated with the median mass diameter (Dm; Petersen *et al.*, 2016). Indeed, the GPM DPR Version 05 single frequency Ku-band rain retrieval algorithm (DPR Algorithm Theoretical Basis Document; https://pmm.nasa.gov/resources/documents/GPM) now uses a global DSD database developed from three-plus years of DPR dual-frequency data. Hamada and Takayabu (2016) indicate that the DPR increases observed precipitation occurrence and volume by 20% and 2%, respectively, between 40˚S and 40˚N with respect to TRMM observations. Battaglia *et al.* (2015) have shown that multiple scattering affects the Ka and Ku radar measurements for deep convective systems and recommended a multiple-scattering forward-operator-based retrieval algorithm, which has since been implemented in the Version 05 CORRA algorithm. A better understanding of the microphysics of falling snow and frozen precipitation above the freezing layer is evolving and the results show that non-spherical particles are essential for radiative transfer modelling simulations in order to match DPR and GMI (across all frequencies) and aircraft data taken during field campaigns (e.g., Kuo *et al.*, 2016; Olson *et al.*, 2016; Molthan and Petersen, 2011).

NASA Author Manuscript

NASA Author Manuscript

NASA Author Manuscript

A calibration transfer standard is facilitated by the highly stable instruments and careful attention to instrument design for the GPM-CO. With regards to the DPR, a diagnosed sidelobe clutter issue was corrected (Kubota *et al.*, 2016), and overall performance demonstrated in Kubota *et al.* (2014), Toyoshima *et al.* (2015) and Iguchi *et al.* (2016). GMI on orbit performance and calibration stability is reported in Draper et *al.* (2015a,b). Subsequently, Wentz and Draper (2016) concluded that GMI is the most accurate precipitation radiometer currently in space. To provide unified global precipitation estimates a reliable transfer standard of brightness temperatures (Tbs) between the GPM-CO and the constellation partner precipitation sensors through the inter-calibration of all the radiometer sensors has been established (Berg *et al.*, 2016). This inter-calibration effort ensures that the observed Tbs are consistent among the sensors allowing for expected differences due to variations in the observing frequencies, bandwidths, polarizations, and view angles (e.g., Wilheit *et al.*, 2015). After inter-calibration, residual differences between the GMI Tbs and those of the constellation radiometers are generally smaller than 1 K (Berg *et al.*, 2016). These GPM inter-calibrated Tbs are made available on the NASA PPS and are the first step toward unified precipitation products.

The second step of the transfer standard uses the combined DPR and GMI CORRA estimates of the GPM-CO to provide a common *a priori* precipitation/radiance database for passive microwave sensor Bayesian retrievals and is key to combining the GPM constellation radiometers into one consistent framework to produce unified global precipitation products (Kummerow *et al.*, 2011). The current GPM-CO combined CORRA radar-radiometer algorithm architecture draws upon a rich heritage of algorithms that were developed for the TRMM mission, as well as other algorithms developed and applied to airborne radar-radiometer data. One of many challenges for the GPM GMI+DPR combined (CORRA) algorithm development is the creation of updated physical parameterizations that enable the algorithm to take better advantage of the Ka radar on the DPR and the higher frequency channels of the GMI (>89 GHz) in order to obtain greater accuracy in the measurement of light rain rates and falling snow. An example of ongoing work demonstrating the GPM-CO multi-instrument active/passive microwave, multi-frequency synergy is shown in Grecu *et al.* (2016) where the precipitation estimates from the combined DPR+GMI CORRA algorithm compared to ground validation data have good correlations but show room for improvement in future versions. Over land, advances have been made by the GPM GPROF algorithm through using GPM ground-validation datasets collected over the U.S. to adjust the GPROF V05 precipitation estimates over snow covered land surfaces. As a result of the GPROF algorithm modification, improvements were noted in GPROF V05 snowfall estimates based on independent comparisons to GV estimates made over the northern mid-latitude continental region of Hyytiälä, Finland (von Lerber *et al.*, 2017).

The third step of the transfer standard uses the combined DPR and GMI CORRA estimates of the GPM-CO to provide a routinely updated calibration for all sensors in the GPM constellation before they are incorporated into the IMERG combined-satellite product. IR-based precipitation estimates used in IMERG are routinely calibrated by the collection of inter-calibrated passive microwave-based precipitation estimates. These two actions ensure that all satellite precipitation estimates used in IMERG have a calibration traceable back to the CORRA product.

NASA Author Manuscript NASA Author Manuscript NASA Author Manuscript

3.2 Contributions to water cycle understanding

Since launch, the DPR 3D measurements, detailed constellation observations, and the IMERG high spatial and temporal resolution merged-data products have provided data on the space-time variability of global precipitation used for scientific research. For example, Liu and Zipser (2015) collected the first year of GPM Ku radar data to classify the largest, deepest, and strongest precipitation systems on Earth. Figure 6 shows the Liu and Zipser (2015) classifications, updated using three years of the Version 05 GPM products (released May 2017). With the higher latitude coverage of the GPM-CO, the DPR confirms that precipitating storm systems in the Great Plains of the U.S. and the Pampas in Argentina are among the most intense on Earth. The largest precipitation systems are found in the mid-latitude extratropical storm tracks, highlighting the role of front in the organization of these larger precipitation systems. Using the DPR dataset Battaglia *et al.* (2016a) found the first evidence of "ghost echoes" which correspond to areas of multiple scattering within the weak-echo regions typically observed by ground-based S-band radar in the vicinity of a tilted convective core of a tornadic supercell. Meanwhile, using GMI microwave polarimetric signals from the vertical and horizontal channels, Gong and Wu (2017) found that the radiative scattering of frozen particles is highly polarized in the upper troposphere throughout the tropics and mid-latitude jet regions, and hence indicate that the ice particles are horizontally oriented. GPM continues to uncover the diversity of phenomena that are both important scientifically and crucial to developing the best retrievals for understanding the water cycle.

3.3 Inputs to hydrological modelling

Downscaling high-resolution precipitation data and innovative hydrological modelling have helped advance predictions of precipitation-related high-impact natural hazard events (e.g., flood, drought, landslide, and hurricanes) and improve hydrological modelling and prediction. GPM and TRMM data have been used to improve quantitative precipitation estimation over land within the U.S. (e.g. Wen *et al.*, 2016; Kirstetter *et al.*, 2015) and internationally (e.g., Libertino *et al.*, 2016). Petkovic and Kummerow (2015) examined the sources of bias in the GMI product, while Tan *et al.* (2016a) compared error sources in IMERG attributable to individual instruments, finding (as expected) that the most reliable IMERG estimates originate from passive microwave estimates. An error model to quantify uncertainty in fine resolution precipitation products for satellite hydrology was proposed by Maggioni *et al.* (2014) and Wright *et al.* (2017). Lin *et al.* (2015) developed a framework for dynamical precipitation downscaling through assimilating 6-h National Centers for Environmental Prediction (NCEP) Stage IV data using the Weather Research and Forecasting (WRF) 4-dimensional (4D)-Varational system. This physically based downscaling methodology can be considered as a proof of concept for the downscaling of fine-scale GPM precipitation observations.

3.4 Efforts toward advancing climate models

Information from GPM's estimates of surface water flux inputs, cloud/precipitation microphysics, convective/stratiform separation, and latent heat release in the atmosphere has the potential for improved parameterization and initialization of climate models (Hagos *et*

NASA Author Manuscript

NASA Author Manuscript

NASA Author Manuscript

al., 2014). Climate models, and their parameterizations within the models, can be verified with global precipitation products but care must be taken to address limitations and enforce quality control (Tapiador *et al.*, 2017). Research using information based upon GPM observations are helping to advance climate and other models that require parameterizations for convection and cloud microphysics. For example, using GPM field campaign data, Adirosi *et al.* (2016) compared raindrop size distributions to modelled size distributions, Tao *et al.* (2013) investigated the diurnal structure of precipitation, while Iguchi *et al.* (2014) used cloud resolving models to study melting-layer structure in mixed-phase precipitation, and Colle *et al.* (2017) viewed the structure and evolution of warm frontal precipitation. Hill et al. (2016) used TRMM data, in conjunction with other satellite data sets, to confirm that the most modern global atmospheric reanalysis (ERA-Interim, produced by European Centre for Medium-Range Weather Forecasts [ECMWF] available from 1979) and global models tend to generate convection too early in the day with consequences for the release of latent heat in south west Africa. More opportunities for studies like this should be possible once GPM calibrates and reprocesses TRMM data, creating a multi-decade record of precipitation.

3.5 Support for improved weather forecasting

GPM's accurate and frequent measurements of precipitation-affected radiances and instantaneous precipitation rates together with quantitative error characterization have been assimilated into weather forecasting and data assimilation systems to improve 4D reanalysis, with the GPM-CO data being used operationally by the ECMWF (Geer *et al.*, 2017). Assimilating satellite observations from microwave imagers such as GMI in cloudy and precipitating regions provides critical constraints on atmospheric parameters in dynamically sensitive regions and makes significant impacts on weather forecast accuracy. Kim *et al.* (2017) describe a framework to assimilate GMI all-sky (including cloud and precipitation affected) radiance data using a hybrid 4D-Ensemble Variational (EnsVar) analysis algorithm in the Goddard Earth Observing System version 5 (GEOS-5) that will become part of NASA's Global Modelling and Assimilation Office (GMAO)'s operational forecast system in 2018.

Zhang *et al.* (2017) have developed an ensemble data assimilation system for the NASA Unified Weather Research and Forecasting (NU-WRF) model, which can optimally integrate the information from high-resolution numerical model predictions and from GPM satellite data. Because precipitation varies greatly in time and space, they have developed an estimation method for forecast errors by using an ensemble of forecasts with optimal perturbations to the initial states of, for instance, temperature, humidity, precipitation, and clouds. The analysis shows an improved representation of monsoon precipitation and its interaction with atmospheric dynamics over West Africa. This assimilation of precipitation-affected microwave radiances impacts the distribution of precipitation intensity and the propagation of cloud-precipitation systems of the African Easterly Jet (Zhang *et al.*, 2017). The Joint Center for Satellite Data Assimilation (JCSDA) is currently testing how GMI data improve track forecasting for tropical cyclones (Kirschbaum *et al.*, 2017; Pu and Yu, 2017).

NASA Author Manuscript NASA Author Manuscript NASA Author Manuscript

4. Ground validation activities and contributions to the GPM mission

GPM GV mission contributions have focused on the collection of high-quality continental scale reference precipitation rate, accumulation and multi-parameter radar datasets; the development and operation of research grade multi-frequency polarimetric radar and precipitation measurement network instrumentation for describing hydrometeor physical characteristics; and the design and implementation of numerous field campaigns consisting of coordinated satellite, ground, and airborne *in situ* and remote sensing data collections that describe liquid, mixed, and ice-phase precipitation types from hydrometeor to satellite sampling scales (Hou *et al.*, 2014). Broadly speaking, these GV contributions have resulted in data suited to long-term direct statistical comparisons between GPM and GV data (e.g., Kirstetter *et al.*, 2012, 2015; Petersen *et al.*, 2016; Tan *et al.*, 2016a,b), as well as datasets from short, more highly targeted field campaigns designed to study precipitation processes and the physical validation of GPM retrieval algorithms (as listed in Table IV).

4.1 GV Ground Instrument Infrastructure

GPM GV has established a world-class inventory of precipitation instrumentation. Equipment developed and operated as part of this instrument suite include the NASA S-band dual-polarization (NPOL) radar (Wolff *et al.*, 2014), the Ku-Ka band Dual-frequency Dual-Polarimetric Doppler Radar (D3R; Vega *et al.*, 2014), numerous Micro Rain Radars (MRR-2; Peters *et al.*, 2002), Pluvio-2 weighing gauges, dense networks of (multiple) tipping bucket rain gauges, snow imaging/measurement systems such as the Precipitation Imaging Package (PIP) (e.g., Newman *et al.*, 2009; Tiira *et al.*, 2016), and autonomously operating Parsivel and 2D Video Disdrometer (2DVD) networks (e.g., Tokay *et al.*, 2017). When not deployed for GPM-related field campaigns, these instruments operate within the NASA Wallops Flight Facility (WFF) network (or partner sites), with special emphasis placed on data collections during GPM-CO overpasses.

4.2 Direct GV Datasets

Considering longer-term statistical validation of GPM satellite products, GV contributions to the mission include two primary multi-parameter datasets (see https://gpm-gv.gsfc.nasa.gov/ for access to these and other GV datasets):

1. *Validation Network (VN) Radar Data:* VN data consist of ~80 U.S. network, oceanic, and/or other national/international research site-specific dual polarimetric (dual-pol) radars that provide derived precipitation rate, DSD and hydrometeor type data that are footprint and column volume-matched to GPM-CO overpasses (Bolen and Chandrasekar, 2003; Schwaller and Morris, 2011). Over 41,000 GPM-VN radar volumes were processed between launch and September 2017 and processing continues. Early VN datasets supported validation of TRMM rainfall rates (e.g., Islam *et al.*, 2012) and checks on surface radar calibration stability in preparation for the GPM-era (e.g., Kim *et al.*, 2014). In the GPM era the aforementioned types of study, now using the DPR instead of TRMM's Precipitation Radar (PR) continue, but the VN has also directly supported verification of mission science requirements (Petersen et al. 2017),

NASA Author Manuscript

NASA Author Manuscript

NASA Author Manuscript

DSD retrieval algorithms (e.g., Grecu *et al.*, 2016), and even studies of GPM hail detection (Leppert and Cecil, 2015).

2. *GV-Multi-Radar Multi-Sensor (MRMS) Precipitation Rates:* GV-MRMS data are rain gauge bias-adjusted radar estimates of precipitation rate and type (rain/snow) for GPM products over the U.S. and neighboring regions (130°−60°W, 20°−55°N). GV-MRMS datasets are derived from NOAA MRMS products (Zhang *et al.*, 2016), but are further processed (e.g., Kirstetter *et al.*, 2012) to produce gauge-corrected reference precipitation intensity datasets augmented with information on precipitation types and data quality at the native temporal (2-minute) and spatial resolution (0.01° × 0.01°) of the MRMS. These products have been used for statistical validation of instantaneous GPM precipitation estimates at individual IFOVs scales (e.g., Kidd *et al.*, 2017b). GV-MRMS data are also used to create 30-minute rain accumulation datasets (including precipitation type, radar quality metrics, etc.) to validate IMERG products (e.g., Tan *et al.*, 2016a,b) and have been integrated with IMERG and field data for hydrologic validation/assimilation studies (e.g., Tao *et al.*, 2016).

4.3 GV Field Campaigns

GPM GV has implemented six major field campaigns (e.g., Figure 3; Table IV), has participated in several targeted international partner-led field campaigns, and conducts ongoing field measurements made at supersites such as WFF. The field measurements focus on a wide range of cold- and warm-season precipitation regimes. Associated datasets (Table IV) include virtually all of the aforementioned ground-based direct-statistical datasets discussed above, but also include high-altitude airborne combinations of radar (W, Ku, Ka, X-band frequencies) and passive microwave radiometer (e.g., 10–183 GHz) remote-sensing data collected from instruments on the NASA DC-8 and/or ER-2 aircraft, airborne *in situ* cloud microphysical measurements, and supporting sounding profiles of atmospheric thermodynamic state.

GV field measurements and related instruments connect GPM satellite-based remote sensing algorithms to column physical processes and precipitation measured at the Earth's surface. The associated data have supported a range of studies related to the testing, development, and/or verification of GPM retrieval algorithms and supporting cloud models. These include the physics of, and methods to parameterize, the DSD (e.g., Williams *et al.*, 2014; Liao *et al.*, 2014; Tokay *et al.*, 2017; Raupach and Berne, 2017), including new observations of small raindrops (< 0.5 mm) and their impact on current approaches to representing the DSD in light rain (Thurai *et al.*, 2017), radar multiple-scattering at DPR frequencies in strong convection (Heymsfield *et al.*, 2013; Battaglia *et al.*, 2016a), and hail signatures in radiometer data (Leppert and Cecil, 2015). Examples of multi-frequency ice and snow scattering studies include Molthan and Petersen (2011), Tyynelä and Chandrasekar (2014), Kneifel *et al.* (2015), and Olson *et al.* (2016), while measurements of snow water equivalent rate can be found in Moisseev *et al.* (2017) and von Lerber *et al.* (2017). GPM's field campaign data have also supported cloud resolving model microphysics (e.g., Shi *et al.*, 2010; Tao *et al.*, 2013; Lang *et al.*, 2014; Colle *et al.*, 2017) and have combined the use of

NASA Author Manuscript NASA Author Manuscript NASA Author Manuscript

hydrologic modelling and observations to develop “best” estimates of liquid and frozen precipitation accumulation over complex terrain (Cao *et al.*, 2017).

In late 2015 and early 2016, GPM GV completed a large field campaign over the mountainous region of the Olympic Peninsula of Washington State, US (OLYMPEX; Houze *et al.*, 2017). In contrast to the warm-season Integrated Precipitation and Hydrology Experiment (IPHEx) campaign that focused primarily on orographic warm-season convective rain (e.g., Table IV), OLYMPEX focused on validation of GPM algorithms and products in cold-season mid-latitude frontal system precipitation (rain and snow) influenced by complex terrain. Indeed, heavy precipitation frequently occurred over the Olympic Mountains with several rain events exceeding 250 mm in 1–2 day time spans along windward slopes. Figure 7 provides one example sampled by ground-based radar, aircraft, and an overpass of the GPM-CO. As evident in Figure 7, orographic perturbation of the prevailing low-level flow and associated enhancements of the precipitation process were important during OLYMPEX (see also Houze *et al.*, 2017, and Zagrodnik *et al.*, 2017). In fact, Figure 7b suggests that orographic enhancements occurring below 2 km (Figs. 7c–d) may be difficult to directly observe using GPM DPR observations. If the enhancement is associated with warm-rain processes, it may also be difficult for radiometers to reliably detect (e.g., Shige and Kummerow, 2016). Indeed, Cao *et al.* (2017) used OLYMPEX measurements and the Variable Infiltration Capacity (VIC) model to develop a composite reference estimate of daily total rain and snow water equivalent at a spatial resolution of 1/32° over the OLYMPEX domain for the October-April 2015–16 time period centered on the experiment. When compared to this reference, it was found that both IMERG and GSMaP underestimated the precipitation by approximately 50% over the higher terrain. From this perspective, detailed analysis of OLYMPEX airborne and ground-based observations will be useful for informing and/or verifying physical processes and estimation uncertainties in GPM retrieval algorithms and associated products in similar frontal/orographic regimes.

Near-term international field efforts such as the International Collaborative Experiment – PyeongChang Olympics-Paralympics 2018 (ICE-POP 2018; led by the Korean Meteorological Administration, February-March, 2018) are enabling further GPM studies of orographic precipitation processes, and in particular, orographic snow, over regions characterized by large ocean to mountain terrain gradients. All GV field campaign datasets are openly available via the Global Hydrology Resource Center Distributed Active Archive Center (DAAC) located at NASA Marshall Space Flight Center (MSFC) (https://ghrc.nsstc.nasa.gov/home/field-campaigns).

5. Applications of GPM data for societal benefit

GPM data provide critical information to end-users that helps to improve our understanding of Earth’s water cycle and facilitates decision-making at local to global scales (Kirschbaum *et al.*, 2017). Building on the legacy of TRMM, the use of high-quality precipitation data provided by GPM, now covering higher latitudes, has enabled new science research and data applications to benefit society across a diverse range of end-users; some examples are shown in Table V and summarized below.

NASA Author Manuscript NASA Author Manuscript NASA Author Manuscript

5.1 Hydrologic modelling, prediction, and water resource management

GPM's instantaneous precipitation products, especially IMERG, are being used as input into hydrological and land surface models. Short-term forecasts of soil moisture and other parameters to better understand the land-atmosphere interactions on scales of days to years are available from the NASA Land Information System (LIS, Kumar *et al.*, 2006) based on GPM and other precipitation data. LIS runs operationally providing data to forecasters in NRT through NASA's Short-term Prediction Research and Transition Center (SPoRT) and SERVIR (Spanish *to serve*) projects (https://weather.msfc.nasa.gov/sport/, https://www.servirglobal.net/).

TRMM and GPM data are being integrated with other rainfall forcing data into the multiagency, multi-national Famine Early Warning System Network (FEWS NET; https://www.fews.net/). IMERG data have been tested within the FEWS NET Land Data Assimilation System to provide information on different agricultural products including the start of the growing season and drought metrics (Kirschbaum *et al.*, 2017). IMERG data have been connected with water resource managers and farmers in the Indus valley though the use of cellphone updates to farmers about when to irrigate their crops (Hossain *et al.*, 2017). GPM has also been important in contributing to food-water-energy dialogues (Shepherd *et al.*, 2016). GPM scientists have analyzed the distribution of the mean precipitation per person (PPP) using IMERG and population density estimates (Figure 8), which highlights the potential water availability and potential water availability stressors coming purely from precipitation (Shepherd *et al.*, 2016). High values are found in areas such as the Amazon basin, western U.S., and Australia, where high precipitation but low populations exist, while areas with dense population, including China and India, have lower PPP. This PPP dataset could lead to several interesting studies such as: Do precipitation regimes (e.g., orographic) affect human habitability? How well can high PPP areas support low PPP areas through water management, agriculture, and/or energy production? What are the direct and indirect costs of these imbalances in global PPP?

5.2 Operational numerical weather and hurricane prediction

To facilitate early use of the GPM-CO data, an informal Early Adopter Program was instituted during the GPM-CO's pre-launch and checkout phases. This early data access allowed the Navel Research Lab (NRL) Automated Tropical Cyclone Forecasting System (https://www.nrlmry.navy.mil/TC.html) to begin integrating GMI data into their system to improve tropical cyclone location fixes the day after the data were released in June 2014 (3 months earlier than planned). As a result, GPM data were used to support tropical cyclone forecasts from the start of the 2014 Atlantic Hurricane season. From June 2014-October 2017, the NRL Tropical Cyclone webpage has recorded nearly 5,000 GMI overpasses of cyclones that have been used by forecasters around the globe to monitor tropical cyclone structure (Dr. Song Yang, personal communication). The GPM-CO DPR provided (3D) data during overpasses of the 2017 Atlantic Hurricane season including the hot towers associated with Hurricanes Harvey, Irma, Jose, Maria, and Ophelia (https://pmm.nasa.gov/extreme-weather/). In addition, GMI data were specifically mentioned in NOAA's National Hurricane Center (NHC) hurricane forecasts for Irma and Jose (National Hurricane Center,

NASA Author Manuscript NASA Author Manuscript NASA Author Manuscript

2017). IMERG has been used to create rainfall accumulation maps from many of the Atlantic (and worldwide) severe storms (e.g., https://svs.gsfc.nasa.gov/4586).

GMI Tb products are operationally assimilated into Numerical Weather Prediction (NWP) models across the globe to improve short- to long-term weather forecasts and correct the track forecasts for tropical cyclones. The Air Force Weather Agency (557th Weather Wing) incorporates GMI data into their WRF model, delivering operational worldwide weather products to the Army and Air Force, unified commands, National Programs, and the National Command Authorities. The JCSDA/NOAA and ECMWF are working to use GPM-CO data within their global NWP model focusing on medium-range (up to two weeks ahead) forecasts; operational inclusion of GPM data into GEOS-5 is expected in 2018. GPM data are also accessed daily by weather prediction agencies around the world including Japan, India, China, Korea, Australia, United Kingdom, France, Brazil, Argentina, Netherlands, among others.

In partnership with the MSFC SPoRT Center, GPM single-channel and multispectral radiometer imagery and rain rate products from all of the satellites in the GPM Constellation are provided to the NHC in a format compatible with their operational National Center for Environmental Prediction (NCEP) Advanced Weather Interactive Processing System (N-AWIPS) decision support system. The satellite liaison at the NHC has confirmed that these data are being ingested into the NHC from SPoRT and noted that integration of the suite of passive microwave imagery (including the GPM-CO) into N-AWIPS has been one of the most significant dataset additions in recent years (Chris Landsea, NHC, personal communication via NASA's SPoRT facility).

5.3 Disaster response, extremes, and disease

Extreme precipitation leading to flood or landslide events, and the characterization of potential hazards, are a source of several GPM investigations (e.g., Petkovic and Kummerow, 2015; Panegrossi *et al.*, 2016; Kirschbaum *et al.*, 2015b). The IMERG spatial and temporal resolutions provide a valuable product to examine precipitation extremes that may result in flooding, landslides, or other meteorologically-induced phenomena and to support disaster response and recovery (Schumann *et al.*, 2016). TRMM and now GPM data are being used in the development and NRT processing of a Global Flood Monitoring System (e.g., Wu *et al.*, 2014) that provides estimates of flood detection, intensity, streamflow, and inundation. Similar work has developed a regional and global Landslide Hazard Assessment model for Situational Awareness (LHASA) that leverage both the long-duration TRMM Multi-satellite Precipitation Analysis (TMPA; Huffman *et al.*, 2007) data and IMERG to provide estimates of potential landslide activity around the world in NRT, as well as to evaluate the coincidence of global landslide data and extreme rainfall patterns (Kirschbaum *et al.*, 2015a). Figure 9 highlights the global distribution of average annual potential landslide activity, which can be used to improve situational awareness of landslide occurrence both spatially and temporally, especially in areas with few ground based observations. The LHASA model is now being run using the Early Run IMERG data (Table III) to provide NRT landslide nowcasts every 30 minutes at 0.1˚ resolution (available at https://pmm.nasa.gov/precip-apps). IMERG estimates are also being used within the Global

NASA Author Manuscript

NASA Author Manuscript

NASA Author Manuscript

Fire WEather Database (GFWED), which integrates different weather factors influencing the likelihood of the initiation and spreading of vegetation fires (Field *et al.*, 2015).

In areas where few rain gauges exist, monitoring or forecasting conditions that can lead to disease vector or water-borne diseases is extremely challenging. Consequently, satellite precipitation estimates, often in NRT, are increasingly becoming the standard precipitation data source in these environments. The IMERG NRT data have been used to track environmental conditions on the ground in order to help predict and validate the risk of cholera infection, for example, as shown in Figure 10 for Haiti immediately after Hurricane Matthew in October, 2016 (Khan *et al.*, 2017). Studies using TRMM have shown that areas of wetter conditions in the higher elevations of Uganda are often associated with increased incidence of Black Plague (Monaghan *et al.*, 2012; MacMillan *et al.*, 2012). TRMM and GPM estimates are also being used to characterize mosquito-breeding habitats in an effort to identify areas with higher disease risk (Valle *et al.*, 2013; Pan *et al.*, 2014; Zaitchik *et al.*, 2014). Research applications will improve with GPM's increased spatiotemporal resolution and accuracy, helping to improve the environmental and climatic conditions for increased disease outbreaks.

6. Conclusions and future prospects

The GPM-CO has proven to be a worthy successor to TRMM, extending and improving high-quality active and passive microwave observations across all times of day with a precessing 65°-inclination orbit. The GPM-CO has provided new insights into sensing snowfall as well as continued innovation across the range of precipitation systems from the Arctic to the Antarctic Circle. The GPM-CO has met its mission success metrics, has set a new standard for passive microwave radiometer accuracy, and has provided the data for processing and disseminating precipitation data for a range of scientific investigations and societal applications. The GPM mission also has provided leadership and the calibration transfer standard (via the GPM-CO) to unify and advance precipitation measurements from a constellation of research and operational sensor data shared by a consortium of domestic and international partners.

The GPM mission is currently in extended operations after successfully completing its end of prime mission review in June 2017 after 3 years on orbit. The GPM-CO has fuel onboard that could last for more than a decade, which provides significant opportunities to continue to maximize the scientific and societal benefits of the mission (contingent on instrument health) by enhancing the understanding of precipitation physical character, processes, structure, and variability from regional to global scales and sub-daily to interannual scales.

In terms of algorithm and products for extended operations, the mission seeks to address the following major topics: lengthen the temporal record by inter-calibrating datasets back to 1998 (for the complete TRMM record, expected release in 2018), extend GPM merged constellation algorithms pole to pole and improve their morphing process, and improve the estimates of falling snow and light rainfall. One critical issue is to improve spaceborne estimates of precipitation over orographic and other complex surface features. In addition, the effects of multiple scattering and non-uniform filling of footprints by precipitation have

NASA Author Manuscript

NASA Author Manuscript

NASA Author Manuscript

not been fully addressed in simulations of radar reflectivities in the DPR and CORRA algorithms, although improved parameterizations are being developed. These effects greatly impact the interpretation of DPR observations at Ka- and Ku-bands.

Scientifically, an extended GPM mission will help to determine inter-annual spatial and temporal variability of global rainfall, hydrometeor and microphysical structure, and associated latent heating for convective systems and storms, and how these characteristics are related to variations in the global water and energy cycles. The longer precipitation record will increase our knowledge of mean precipitation variations and intensity distributions from inter-annual to multi-decadal time scales by utilizing the increased sampling statistics, accuracy, and passive/active synergy of the GPM and TRMM observations, by linking this recent period to earlier observations and by validating modelling results from emerging high-resolution climate models.

New GPM science investigations fall into the following themes: (1) research on microphysics and physical properties of precipitation systems observed by the GPM-CO, including the characterizations of extreme events; (2) long-term precipitation datasets that will permit global precipitation and circulation pattern investigations, including their variability in terms of ENSO and other global time variations; and (3) the development of fine-scale regional climatologies of precipitation characteristics (mean surface rain, diurnal cycle, vertical structure) on a monthly to seasonal basis. Through assimilation and other methods, the U.S. GPM project plans to develop a national precipitation product based on modelling that reproduces GPM precipitation statistics at the time and space scales of the observations, but also defines higher resolution (downscaled) information for scientific studies and applied uses.

New research might include studies of other retrievable products (such as winds and surface emissivity) from the GPM datasets, more detailed estimates of latent heating in the mid-latitudes, improved estimates of light rain, and better assessments of falling snow properties. Early work has shown that ocean wind speeds are retrievable from GPM data (Munchak *et al.*, 2016; Nouguier *et al.*, 2016) but require verification through additional scientific investigations and validation efforts. Enhancement of land and ocean surface emissivity/ radar cross section retrievals (e.g., Prigent *et al.*, 2015; Tian *et al.*, 2013; Ferraro *et al.*, 2013; Harrison *et al.*, 2016; Turk *et al.* 2014) is important because these are vital environmental conditions required by the precipitation retrieval algorithms, especially as the algorithms move toward more physically based descriptions of surface properties (e.g., Kummerow *et al.*, 2015). Other research in process involves extending the TRMM Latent Heating dataset to the mid-latitudes, where the organization of mid-latitude cyclones is vastly different than that of convective systems in the tropics (Liu and Liu, 2016; Liu and Zipser, 2015). Scientific investigations are required to assess the differences of latent heat structure in stratiform and convective precipitation regions in the mid-latitudes, and to address what defines these structures at these latitudes.

TRMM has shown the value of a long record of precipitation in many science inquiries (e.g., Curtis *et al.*, 2007; Lau and Wu, 2010; Liu *et al.*, 2015). GPM will expand this record and, in addition, because of the increased mid-latitude coverage of the GPM-CO compared to

NASA Author Manuscript NASA Author Manuscript NASA Author Manuscript

TRMM, scientific investigations are planned for these higher latitudes. For example, the GPM-CO can now track tropical cyclones as they become extra-tropical and can help identify corresponding changes in precipitation characteristics as storm structure changes at higher latitudes and permits coordinated observational and modelling studies on storm intensity and precipitation. The GPMCO is the first NASA satellite capable of measuring moderate and heavy snowstorms in detail. In particular, the 3D capabilities of DPR bring new space-based capabilities for studying classical Nor'easters and other extratropical storms in the northern or southern hemispheres.

A key contribution to the community will be the retrospective processing of the U.S. team's IMERG back to 2000, which will be released to the public in 2018. These datasets will provide the first-ever fine-scale record of quasi-global precipitation for nearly two decades computed with the next-generation GPM-based algorithms. Continued computation of near-real-time and high quality research estimates will benefit society though improvement across a range of application and operational activities, including storms, floods, landslides, droughts, agricultural forecasting, and water resource management. Taken together, these initiatives will continue to exploit the potential of the GPM-CO and constellation to advance precipitation science and address societal needs in the coming years. Indeed, GPM's precipitation observations are key to addressing World Climate Research Program (WCRP) research challenges by providing data for scientific studies such as improving our knowledge of atmospheric circulation patterns, defining precipitation's role in climate sensitivity, cataloging weather extremes, assessing precipitation inputs for the world's agricultural food baskets, and providing key observations that refine modelling assumptions about precipitation, thus improving climate prediction.

Acknowledgements

Thanks go to Lisa Milani (National Research Council of Italy/Michigan Technical University) for the CloudSat/DPR difference images of Figure 5; Stephanie Wingo (NASA MSFC/USRA) for contributions to Figure 7; Chuntao Liu (Texas A&M) and Marshall Shepherd (University of Georgia) for Figure 8, and Antar Jutla (West Virginia University) for Figure 10. Thanks also go to, Pierre Kirstetter (NOAA/National Severe Storms Laboratory) for MRMS processing and related research, and Lisa Nalborczyk (NASA Goddard Space Flight Center) for helping with editing. Our three anonymous reviewers provided valuable feedback. We also thank NASA's Precipitation Measurement Mission science team and international partners (https://pmm.nasa.gov/PMM-science-team), as well as the international GV teams for their excellent support.

8. References

Adirosi E, Volpi E, Lombardo F, Baldini L, 2016 Raindrop size distribution: Fitting performance of common theoretical models. Adv. Water Res 96 : 290–305. DOI: 10.1016/j.advwatres.2016.07.010

Aonashi K, Awaka J, Hirose M, Kozu T, Kubota T, Liu GS, Shige S, Kida S, Seto S, Takahashi N, Takayabu YN, 2009 GSMaP Passive Microwave Precipitation Retrieval Algorithm: Algorithm Description and Validation. J. Meteorol. Soc. Japan 87A : 119–136. DOI: 10.2151/jmsj.87A.119

Arndt DS, Baringer MO, Johnson MR. 2010 State of the climate in 2009. Bull. Amer. Meteor. Soc 91 : s1–s222. DOI: 10.1175/BAMS-91-7-StateoftheClimate

Barros AP, Petersen W, Schwaller M, Cifelli R, Mahoney K, Peters-Liddard C, Shepherd M, Nesbitt S, Wolff D, Heymsfield G, Starr D. 2014 NASA GPM-Ground Validation: Integrated Precipitation and Hydrology Experiment 2014 Science Plan. EPL/Duke University (Pub.): 64pp. 10.7924/G8CC0XMR

NASA Author Manuscript NASA Author Manuscript NASA Author Manuscript

Battaglia A, Mroz K, Tanelli S, Tridon F, Kirstetter PE. 2016a Multiple-Scattering-Induced "Ghost Echoes" in GPM DPR Observations of a Tornadic Supercell. J. Appl. Meteor. Climatol 55 : 1653–1666. DOI: 10.1175/JAMC-D-15-0136.1

Battaglia A, Mroz K, Lang T, Tridon F, Tanelli S, Tian L, Heymsfield GM. 2016b Using a multiwavelength suite of microwave instruments to investigate the microphysical structure of deep convective core. J. Geophys. Res 121 : 9356–9381. DOI: 10.1002/2016JD025269

Battaglia A, Tanelli S, Mroz K, Tridon F, 2015 Multiple scattering in observations of the GPM dual-frequency precipitation radar: Evidence and impact on retrievals. J. Geophys. Res 120 : 4090–4101. DOI: 10.1002/2014JD022866

Battaglia A, Tanelli S, Heymsfield GM, Tian L. 2014 The Dual Wavelength Ratio Knee: A Signature of Multiple Scattering in Airborne Ku–Ka Observations. J. Appl. Meteor. Climatol 53 : 1790–1808. DOI: 10.1175/JAMC-D-13-0341.1

Berg W, Bilanow S, Chen R, Datta S, Draper D, Ebrahimi H, Farrar S, Jones WL, Kroodsma R, McKague D, Payne V, Wang J, Wilheit T, Yang JX. 2016 Intercalibration of the GPM Radiometer Constellation. J. Atmos. Oceanic Technol. 33 : 2639–2654. DOI: 10.1175/JTECHD-16-0100

Bolen S, Chandrasekar V. 2003 Methodology for aligning and comparing spaceborne radar and ground-based radar observations. J. Atmos. Oceanic Technol 20 : 647–659. DOI: 10.1175/1520-0426(2003)20<647:MFAACS>2.0.CO;2

Cao Q, Painter TH, Currier WH, Lundquist JD, Lettenmaier DP, 2017: Estimation of precipitation over the OLYMPEX domain during winter 2015–16. J. Hydrometeor, accepted.

Casella D, Panegrossi G, San P, Marra AC, Dietrich S, Johnson BT, Kulie MS. 2017 Evaluation of the GPM-DPR Snowfall Detection Capability: Comparison with CloudSat-CPR. Atmos. Res. 197 : 64–75. DOI: 10.1016/j.atmosres.2017.06.018

Chambon P, Zhang SQ, Hou AY, Zupanski M, Cheung S. 2014 Assessing the impact of preGPM microwave precipitation observations in the Goddard WRF ensemble data assimilation system. Quart. J. Roy. Meteorol. Soc 140 : 1219–1235. DOI: 10.1002/qj.2215

Colle BA, Naeger AR, Molthan A. 2017 Structure and Evolution of a Warm Frontal Precipitation Band during the GPM Cold Season Precipitation Experiment (GCPEx). Mon. Wea. Rev 145 : 473–493. DOI: 10.1175/MWR-D-16-0072.1

Curtis S, Salahuddin A, Adler RF, Huffman GJ, Gu G, Hong Y. 2007 Precipitation Extremes Estimated by GPCP and TRMM: ENSO Relationships. J. Hydromet 8 : 678–689. DOI: 10.1175/JHM601.1

Draper DW, Newell DA, Wentz FJ, Krimchansky S, Skofronick-Jackson S. 2015a The Global Precipitation Measurement (GPM) Microwave Imager (GMI): Instrument Overview and Early On-orbit Performance. IEEE Journal of Selected Topics in Applied Earth Observations and Remote Sensing. 8 : 3452–3462. DOI: 10.1109/JSTARS.2015.2403303

Draper DW, Newell DA, McKague DS, Piepmeier JR. 2015b Assessing Calibration Stability Using the Global Precipitation Measurement (GPM) Microwave Imager (GMI) Noise Diodes. IEEE Journal of Selected Topics in Applied Earth Observations and Remote Sensing. 8 : 4239–4247. DOI: 10.1109/JSTARS.2015.2406661

Ferraro R, Peters-Lidard CD, Hernandez C, Turk FJ, Aires F, Prigent C, Lin X, Boukabara SA, Furuzawa FA, Gopalan K, Harrison KW, Karbou F, Li L, Liu C, Masunaga H, Moy L, Ringerud S, Skofronick-Jackson GM, Tian Y, Wang NY. 2013 An Evaluation of Microwave Land Surface Emissivities over the Continental United States to Benefit GPM-Era Precipitation Algorithms. IEEE Trans. Geoscience and Remote Sensing (TGARS). 51 : 378–398. DOI: 10.1109/TGRS.2012.2199121

Field PR, Heymsfield AJ. 2015 Importance of snow to global precipitation. Geophys. Res. Lett. 42 : 9512–9520. DOI:10.1002/2015GL065497. 10.1002/2015GL065497.

Field RD, Spessa AC, Aziz NA, Camia A, Cantin A, Carr R, De Groot WJ, Dowdy AJ. 2015 Development of a Global Fire Weather Database. Nat. Hazards Earth Syst. Sci 15 : 1407–1423. DOI: 10.5194/nhess-15-1407-2015

Geer AJ, Baordo F, Bormann N, Chambon P, English SJ, Kazumori M, Lawrence H, Lean P, Lonitz K, Lupu C. 2017 The growing impact of satellite observations sensitive to humidity, cloud and precipitation. Q. J. R. Meteorol. Soc DOI: 10.1002/qj.3172

NASA Author Manuscript NASA Author Manuscript NASA Author Manuscript

Gong J, Wu DL. 2017 Microphysical Properties of Frozen Particles Inferred from Global Precipitation Measurement (GPM) Microwave Imager (GMI) Polarimetric Measurements. Atmos. Chem. Phys 17 : 2741–2757. 10.5194/acp-17-2741-2017

Grecu M, Olson WS, Munchak SJ, Ringerud S, Liao L, Haddad Z, Kelley BL, McLaughlin SF. 2016 The GPM Combined Algorithm. J. Atmos. Oceanic Technol 33 : 2225–2245. DOI: 10.1175/JTECH-D-16-0019.1

Hagos S, Feng Z, Burleyson CD, Lim K-SS, Long CN, Wu D, and Thompson G 2014: Evaluation of convection-permitting model simulations of cloud populations associated with the Madden-Julian Oscillation using data collected during the AMIE/DYNAMO field campaign, J. Geophys. Res. Atmos, 119, 12,052–12,068, doi:10.1002/2014JD022143.

Hamada A, Takayabu YN. 2016 Improvements in Detection of Light Precipitation with the Global Precipitation Measurement Dual-Frequency Precipitation Radar (GPM DPR). J. Atmos. Oceanic Technol 33 : 653–667. DOI: 10.1175/JTECH-D-15-0097.1

Harrison KW, Tian Y, Peters-Lidard C, Ringerud S, Kumar SV. 2016 Calibration to Improve Forward Model Simulation of Microwave Emissivity at GPM Frequencies Over the U.S. Southern Great Plains. IEEE Transactions on Geoscience and Remote Sensing. 54 : 1103–1117. DOI: 10.1109/TGRS.2015.2474120 [PubMed: 29795962]

Heymsfield GM, Tian L, Li L, McLinden M, Cervantes JI. 2013 Airborne Radar Observations of Severe Hailstorms: Implications for Future Spaceborne Radar. J. Appl. Meteor. Climatol 52 : 1851–1867. DOI: 10.1175/JAMC-D-12-0144.1

Hill PG, Allan RP, Chiu JC, Stein THM. 2016 A multisatellite climatology of clouds, radiation, and precipitation in southern West Africa and comparison to climate models. J. Geophys. Res 121 : 10,857–10,879. DOI: 10.1002/2016JD025246

Hossain F, Biswas N, Ashraf M, and Zeeshan BA, 2017: Growing More with Less in the Indus Valley Using Cellphones and Satellite Data. Eos. 98 : 1–12, 10.1029/2017EO075143

Hou AY, Kakar RK, Neeck S, Azarbarzin AA, Kummerow CD, Kojima M, Oki R, Nakamura K, Iguchi T. 2014 The Global Precipitation Measurements Mission. Bull. Amer. Meteor. Soc 95 : 701–722. DOI: 10.1175/BAMS-D-13-00164.1

Houze RA, McMurdie L, Petersen WA, Schwaller MR, Baccus W, Lundquist J, Mass C, Nijssen B, Rutledge SA, Hudak D, Tanelli S, Mace GG, Poellot M, Lettenmaier D, Zagrodnik J, Rowe A, DeHart J, Madaus L, Barnes H. 2017 The Olympic Mountains Experiment (OLYMPEX). Bull. Amer. Meteorol. Soc DOI: 10.1175/BAMS-D-16-0182.1

Huffman GJ, Adler RF, Bolvin DT, Gu G, Nelkin EJ, Bowman KP, Hong Y, Stocker EF, Wolff DB. 2007 The TRMM Multi-satellite Precipitation Analysis: Quasi-Global, Multi-Year, Combined-Sensor Precipitation Estimates at Fine Scale. J. Hydrometeor 8: 38–55. DOI: 10.1175/JHM560

Huffman GJ, Bolvin DT, Braithwaite D, Hsu K, Joyce R, Kidd C, Nelkin EJ, Sorooshian S, Tan J, Xie P. 2017 Algorithm Theoretical Basis Document (ATBD) Version 4.6 for the NASA Global Precipitation Measurement (GPM) Integrated Multi-satellitE Retrievals for GPM (IMERG). 32pp. GPM Project: Greenbelt, MD [Available online at https://pmm.nasa.gov/sites/default/files/document_files/IMERG_ATBD_V4.6.pdf]

Iguchi T, Seto S, Awaka J, Meneghini R, Kubota T, Chandra V, Yoshida N, Kawamoto N, Oki R. 2016 Precipitation rates estimated with GPM's Dual-frequency Radar. Proc. IEEE Int. Conf. on Geoscience and Remote Sensing Symp. 2016, Beijing, China, 10–15 July 2016 3917–3918pp. DOI: 10.1109/IGARSS.2016.7730017

Iguchi T, Matsui T, Tao WK, Khain AP, Phillips VTJ, Kidd C, L'Ecuyer T, Braun SA, Hou A. 2014 WRF–SBM Simulations of Melting-Layer Structure in Mixed-Phase: Precipitation Events Observed during LPVEx. J. Appl. Meteor. Climatol 53 : 2710–2731. DOI: 10.1175/JAMC-D13-0334.1

IPCC, 2014: Climate Change 2014: Synthesis Report. Contribution of Working Groups I, II and III to the Fifth Assessment Report of the Intergovernmental Panel on Climate Change [Core Writing Team, Pachauri RK and Meyer LA (eds.)]. IPCC, Geneva, Switzerland, 151 pp.

Islam T, Rico-Ramirez MA, Han D, Srivastava PK, Ishak AM. 2012 Performance evaluation of the TRMM precipitation estimation using ground-based radars from the GPM validation network. J. Atmos. Solar. Terrestrial Phys. 77 : 194–208. DOI: 10.1016/j.jastp.2012.01.001

NASA Author Manuscript NASA Author Manuscript NASA Author Manuscript

Jensen MP, Petersen WA, Bansemer A, Bharadwaj N, Carey LD, Cecil DJ, Collis SM, Del Geneio AD, Dolan B, Gerlach J, Giangrande SE, Heymsfield A, Heymsfield G, Kollias P, Lang TJ, Nesbitt SW, Neumann A, Poellot M, Rutledge SA, Schwaller M, Tokay A, Williams CR, Wolff DB, Xie S, Zipser EJ. 2016 The Midlatitude Continental Convective Clouds Experiment (MC3E). Bull. Amer. Meteor. Soc 97 : 1667–1686. DOI: 10.1175/BAMS-D-14-00228.1

Khan R, Anwar R, Akanda A, McDonald MD, Huq A, Jutla A, Colwell R. 2017 Assessment of Risk of Cholera in Haiti following Hurricane Matthew. American Journal of Tropical Medicine and Hygiene. DOI: 10.4269/ajtmh.17-0048

Kidd C, Huffman GJ, Becker A, Skofronick-Jackson G, Kirschbaum D, Joe P, Muller C, 2017a So, how much of the Earth's surface is covered by rain gauges? Bull. Amer. Meteor. Soc 98 : 69–78. DOI: 10.1175/BAMS-D-14-00283.1

Kidd C, Tan J, Kirstetter P-E, Petersen WA, 2017b: Validation of the Version 05 Level 2 precipitation products from the GPM Core Observatory and constellation satellite sensors. Q. J. R. Meteorol. Soc. First Published: 4 12 10.1002/qj.3175

Kidd C, Dawkins E, Huffman G. 2013 Comparison of Precipitation Derived from the ECMWF Operational Forecast Model and Satellite Precipitation Datasets. J. Hydrometeor 14 : 1463–1482. DOI: 10.1175/JHM-D-12-0182.1

Kim M, Todling R, Gelaro R. 2017 Assimilation of All-sky GPM Microwave Imager (GMI) radiance data in NASA GEOS-5 model. Part I: Implementation. Mon. Wea. Rev, Accepted.

Kim J, Ou M, Park J, Morris KR, Schwaller MR, Wolff DB. 2014 Global Precipitation Measurement (GPM) Ground Validation (GV) Prototype in the Korean Peninsula. J. Atmos. Oceanic Technol 31 : 1902–1921. DOI: 10.1175/JTECH-D-13-00193.1

Kim JE, Alexander MJ. 2013 Tropical Precipitation Variability and Convectively Coupled Equatorial Waves on Submonthly Time Scales in Reanalyses and TRMM. J. Climate 26 : 3013–3030. DOI: 10.1175/JCLI-D-12-00353.1

Kirschbaum DB, Huffman GJ, Adler RF, Braun S, Garrett K, Jones E, McNally A, SkofronickJackson G, Stocker E, Wu H, Zaitchik BF. 2017 NASA's Remotely-sensed Precipitation: A Reservoir for Applications Users. Bull. Am. Meteorol. Soc 98 : 1169–1184. DOI: 10.1175/BAMS-D-15-00296.1

Kirschbaum DB, Patel K. 2016 Precipitation data key to food security and public health. EOS, [Available online at https://eos.org/meeting-reports/precipitation-data-key-to-food-security-andpublic-health]

Kirschbaum D, Stanley T, Zhou Y. 2015a Spatial and temporal analysis of a global landslide catalog. Geomorphology. 249 : 4–15. DOI: 10.1016/j.geomorph.2015.03.016

Kirschbaum DB, Stanley T, Simmons J. 2015b A dynamic landslide hazard assessment system for Central America and Hispaniola. Nat. Hazards Earth Syst. Sci 15 : 2257–2272. DOI: 10.5194/nhess-15-2257-2015

Kirstetter PE, Hong Y, Gourley JJ, Schwaller M, Petersen W, Cao Q. 2015 Impact of sub-pixel rainfall variability on spaceborne precipitation estimation: evaluating the TRMM 2A25 product. Q. Journal of the Royal Met. Soc 141 : 953–966. DOI: 10.1002/qj.2416

Kirstetter P, Hong Y, Gourley JJ, Chen S, Flamig ZL, Zhang J, Schwaller M, Petersen W, Amitai E. 2012 Toward a framework for systematic error modelling of spaceborne precipitation radar with NOAA/NSSL ground radar-based National Mosaic QPE. J. Hydrometeor 13 : 1285–1300. DOI: 10.1175/JHM-D-11-0139.1

Kneifel S, von Lerber A, Tiira J, Moisseev D, Kollias P, Leinonen J. 2015 Observed relations between snowfall microphysics and triple-frequency radar measurements: Triple frequency signatures of snowfall. J. Geophys. Res 120 : 6034–6055. DOI: 10.1002/2015JD023156

Kubota T, Yoshida N, Urita S, Iguchi T, Seto S, Meneghini R, Awaka J, Hanado H, Kida S, Oki R. 2014 Evaluation of Precipitation Estimates by at-Launch Codes of GPM/DPR Algorithms Using Synthetic Data from TRMM/PR Observations. IEEE Journal of Selected Topics in Applied Earth Observations and Remote Sensing. 7 : 3931–3944. DOI: 10.1109/JSTARS.2014.2320960

Kubota T, Iguchi T, Kojima M, Liao L, Masaki T, Hanado H, Meneghini R, Oki R. 2016 A Statistical Method for Reducing Sidelobe Clutter for the Ku-Band Precipitation Radar on board the GPM Core Observatory. J. Atmos. Oceanic Technol 33: 1413–1428. DOI:10.1175/JTECHD-15-0202.1

NASA Author Manuscript NASA Author Manuscript NASA Author Manuscript

Kucera PA, Ebert EE, Turk FJ, Levizzani V, Kirschbaum D, Tapiador FJ, Loew A, Borsche M. 2013 Precipitation from space: Advancing Earth system science. Bull. Amer. Meteor. Soc 94 : 365–375. DOI: 10.1175/BAMS-D-11-00171.1

Kumar SV, Peters-Lidard CD, Tian Y, Houser PR, Geiger J, Olden S, Lighty L, Eastman JL, Doty B, Dirmeyer P, Adams J, Mitchell K, Wood EF, Sheffield J. 2006 Land Information System - An Interoperable Framework for High Resolution Land Surface Modelling. Environ. Model. Softw 21 : 1402–1415, [Available online at www.sciencedirect.com]

Kummerow CD, Randel DL, Kulie M, Wang NY, Ferraro R, Munchak SJ, Petkovic V. 2015 The Evolution of the Goddard Profiling Algorithm to a Fully Parametric Scheme. J. Atmos. Oceanic Technol 32 : 2265–2280. DOI: 10.1175/JTECH-D-15-0039.1

Kummerow CD, Ringerud S, Crook J, Randel D, Berg W. 2011 An observationally generated apriori database for microwave rainfall retrievals. J. Atmos. Oceanic Technol 28 : 113–130. DOI: 10.1175/2010JTECHA1468.1

Kummerow C, Simpson J, Thiele O, Barnes W, Chang ATC, Stocker E, Adler RF, Hou A, Kakar R, Wentz F, Ashcroft P, Kozu T, Hong Y, Okamoto K, Iguchi T, Kuroiwa H, Im E, Haddad Z, Huffman G, Ferrier B, Olson WS, Zipser E, Smith EA, Wilheit TT, North G, Krishnamurti T, Nakamura K. 2000 The Status of the Tropical Rainfall Measuring Mission (TRMM) after Two Years in Orbit. J. Appl. Meteorol 39 : 1965–1982. DOI: 10.1175/15200450(2001)040<1965:TSOTTR>2.0.CO;2

Kuo KS, Olson WS, Johnson BT, Grecu M, Tian L, Clune TL, van Aartsen BH, Heymsfield AJ, Liao L, Meneghini R. 2016 The Microwave Radiative Properties of Falling Snow Derived from Nonspherical Ice Particle Models. Part I: An extensive database of simulated pristine crystals and aggregate particles, and their scattering properties, J. Appl. Meteor. Climatol 55 : 691–708. DOI: 10.1175/JAMC-D-15-0130.1

Lau KM, Wu HT. 2010 Characteristics of precipitation, cloud, and latent heating associated with the Madden–Julian Oscillation. J. Climate 23 : 504–518. DOI: 10.1175/2009JCLI2920.1

Leppert KD, Cecil DJ. 2015 Signatures of Hydrometeor Species from Airborne Passive Microwave Data for Frequencies 10–183 GHz. J. Appl. Meteor. Climatol 54 : 1313–1334. DOI: 10.1175/JAMC-D-14-0145.1

Liao L, Meneghini R, Tokay A. 2014 Uncertainties of GPM DPR Rain Estimates Caused by DSD Parameterizations. J. Appl. Meteor. Climatol 53 : 2524–2537. DOI: 10.1175/JAMC-D14-0003.1

Libertino A, Sharma A, Kalshmi V, Claps P. 2016 A global assessment of the timing of extreme rainfall from TRMM and GPM for improving hydrologic design. Environmental Research Letters, 11 : 054003 DOI: 10.1088/1748-9326/11/5/054003

Lin LF, Ebtehaj AM, Bras RL, Flores AN, Wang J. 2015 Dynamical Precipitation Downscaling for Hydrologic Applications Using WRF 4D-Var Data Assimilation: Implications for GPM Era. J. Hydrometeor 16 : 811–829. DOI: 10.1175/JHM-D-14-0042.1

Liu C, Shige S, Takayabu Y, Zipser E. 2015 Latent Heating Contribution from Precipitation Systems with Different Sizes, Depths, and Intensities in the Tropics. J. Climate 28 : 186–203. DOI: 10.1175/JCLI-D-14-00370.1

Liu C, Zipser EJ. 2015 The global distribution of largest, deepest, and most intense precipitation systems. Geophys. Res. Lett 42 : 3591–3595. DOI: 10.1002/2015GL063776

Liu C, Zipser EJ. 2009 “Warm Rain” in the tropics: seasonal and regional distributions based on 9 yr. of TRMM data. J. Climate 22 : 767–779. DOI: 10.1175/2008JCLI2641.1

Liu N, Liu C. 2016 Global distribution of deep convection reaching tropopause in 1 year GPM observations. J. Geophys. Res 121 : 3824–3842. DOI: 10.1002/2015JD024430

Liu WT, Xie X. 2017 Pre-monsoon drought in India observed from space. J. of Hydrometeor 18 : 683–692. DOI: 10.1175/JHM-D-16-0014.1

MacMillan K, Monaghan AJ, Apangu T, Griffith KS, Mead PS, Acayo S, Acidri R, Moore SM, Mpanga JT, Enscore RE, Gage KL, Eisen RJ. 2012 Climate predictors of the spatial distribution of human plague cases in the West Nile region of Uganda. Am. J. Trop. Med. Hyg 86 : 514–523. DOI: 10.4269/ajtmh.2012.11-0569 [PubMed: 22403328]

NASA Author Manuscript NASA Author Manuscript NASA Author Manuscript

Maggioni V, Sapiano MRP, Adler RF, Tian Y, Huffman GJ. 2014 An Error Model for Uncertainty Quantification in High-Time-Resolution Precipitation Products. J. Hydrometeor 15 : 1274–1292. DOI: 10.1175/JHM-D-13-0112.1

Masaki T, Kubota T, Oki R, Furukawa K, Kojima M, Miura T, Iguchi T, Hanado H, Kai H, Yoshida N, Higashiuwatoko T. 2015 Current status of GPM/DPR level 1 algorithm development and DPR calibration. Proc. IEEE Int. Conf. on Geoscience and Remote Sensing Symp. 2015, Milan, Italy 2615–2618. DOI: 10.1109/IGARSS.2015.7326348.

Moisseev D, von Lerber A, Tiira J. 2017 Quantifying the effect of riming on snowfall using ground-based observations. J. Geophy. Res. Atmos 122 : 4019–4037 DOI: 10.1002/2016JD026272

Molthan A, Petersen WA. 2011 Incorporating Ice Crystal Scattering Databases in the Simulation of Millimeter Wavelength Radar Reflectivity. J. Atmos. Ocean Tech 26 : 2257–2269. DOI: 10.1175/2010JTECHA1511.1

Monaghan AJ, MacMillan K, Moore SM, Mead PS, Hayden MH, Eisen RJ. 2012 A regional climatography of West Nile, Uganda, to support human plague modelling. J. Appl. Meteorol. Climatol 51 : 1201–1221. DOI: 10.1175/JAMC-D-11-0195.1

Munchak SJ, Meneghini R, Grecu M, Olson WS. 2016 A Consistent Treatment of Microwave Emissivity and Radar Backscatter for Retrieval of Precipitation over Water Surfaces. J. Atmos. Oceanic. Technol 33 : 215–229. DOI: 10.1175/JTECH-D-15-0069.1

Munchak SJ, Skofronick-Jackson G. 2012 Evaluation of precipitation detection over various surfaces from passive microwave imagers and sounders. Atmos. Res 131 : 81–94. DOI: 10.1016/j.atmosres.2012.10.011

National Hurricane Center, 2017 http://www.nhc.noaa.gov/archive/2017/al12/al122017.discus.024.shtml?http://www.nhc.noaa.gov/archive/2017/al11/al112017.discus.037.shtml? (accessed Nov 14, 2017)

National Research Council, 2013 Climate and social stress: implications for security analysis. National Academies Press.

Newman A, Kucera P, Bliven L. 2009 Presenting the Snowflake Video Imager (SVI). J. Atmos. Oceanic Tech 26 : 167–179. DOI: 10.1175/2008JTECHA1148.1

Nouguier F, Mouche A, Rascle N, Chapron B, Vandemark D. 2016 Analysis of Dual-Frequency Ocean Backscatter Measurements at Ku- and Ka-Bands Using Near-Nadir Incidence GPM Radar Data. IEEE Geoscience and Remote Sensing Letters. 13 : 1310–1314. DOI: 10.1109/LGRS.2016.2583198

Olson WS, Tian L, Grecu M, Kuo KS, Johnson BT, Heymsfield AJ, Bansemer A, Heymsfield GM, Wang JR, Meneghini R. 2016 The Microwave Radiative Properties of Falling Snow Derived from Nonspherical Ice Particle Models. Part II: Initial Testing Using Radar, Radiometer and In Situ Observations. J. Appl. Meteor. Climatol 55 : 709–722. DOI: 10.1175/JAMC-D-150131.1

Pan W, Branch O, Zaitchik B. 2014 Impact of climate change on vector-borne disease in the amazon Global Climate Change and Public Health, Springer, New York 7 : 193–210. DOI: 10.1007/978-1-4614-8417-2_11

Panegrossi G, Casella D, Dietrich S, Marra AC, Sanó P, Mugnai A, Baldini L, Roberto N, Adirosi E, Cremonini R, Bechini R, Vulpiani G, Petracca M, Porcù. 2016 Use of the GPM Constellation for Monitoring Heavy Precipitation Events Over the Mediterranean Region. IEEE Journal of Selected Topics in Applied Earth Observations and Remote Sensing. 9 : 2733–2753. DOI: 10.1109/JSTARS.2016.2520660

Peters G, Fischer B, Andersson T, 2002: Rain observations with a vertically-looking Micro Rain Radar (MRR). Boreal Env. Res, 7, 353–362.

Petersen WA, Houze RA, McMurdie L, Zagrodnik J, Tanelli S, Lundquist J, Wurmann J. 2016 The Olympic Mountains Experiment (OLMPEX): From Ocean to Summit. Meteorol. Tech. Int'l Vol. Sept. 2016 : 22–26pp.

Petersen WA, Huffman G, Kidd C, Skofronick-Jackson G. 2017 Ground Validation Assessments of GPM Core Observatory Science Requirements. European Geophysical Union, General Assembly, Vienna, Austria 23–28 4, 2017.

Petkovic V, Kummerow CD. 2015 Performance of the GPM Passive Microwave Retrieval in the Balkan Flood Event of 2014. J. Hydrometeor 16 : 2501–2518. DOI: 10.1175/JHM-D-15-0018.1

NASA Author Manuscript NASA Author Manuscript NASA Author Manuscript

Prigent C, Liang P, Tian Y, Aires F, Moncet JL, Boukabara SA. 2015 Evaluation of modelled microwave land surface emissivities with satellite-based estimates. J. Geophys. Res 120 : 2706–2718. DOI: 10.1002/2014JD021817

Pu Z and Yu C. 2017 Assimilation of GPM Microwave Imager Clear-Sky Radiance in improving Hurricane Forecasts. Joint Center for Satellite Data Assimilation Quarterly, No. 57, 10.7289/V50P0X8R

Rasmussen R, Baker B, Kochendorfer J, Meyers T, Landolt S, Fischer AP, Black J, Thériault JM, Kucera P, Gochis D, Smith C, Nitu R, Hall M, Ikeda K, Gutmann E. 2012 How Well Are We Measuring Snow: The NOAA/FAA/NCAR Winter Precipitation Test Bed. Bull. Amer. Meteor. Soc 93 : 811–829. DOI: 10.1175/BAMS-D-11-00052.1

Raupach T, Berne A. 2017 Invariance of the double-moment normalized raindrop size distribution through 3D spatial displacement in stratiform rain. J. Appl. Meteorol. Clim 56 : 1663–1680. DOI: 10.1175/JAMC-D-16-0316.1

Reed PM, Chaney NW, Herman JD, Ferringer MP, Wood EF. 2015 Internationally coordinated multi-mission planning is now critical to sustain the space-based rainfall observations needed for managing floods globally. Environ. Res. Lett 10 : 024010 DOI: 10.1088/17489326/10/2/024010

Schäfer SAK, Hogan RJ, Klinger C, Chiu JC, Mayer B. 2016 Representing 3-D cloud radiation effects in two-stream schemes: 1. Longwave considerations and effective cloud edge length. J. Geophys. Res 121 : 8567–8582. DOI: 10.1002/2016JD024876

Schumann G, Kirschbaum D, Anderson E, Rashid K. 2016 Role of Earth Observation Data in Disaster Response and Recovery: From Science to Capacity Building. Earth Science Satellite Applications: Current and Future Prospects. Hossain F, Ed., Springer Remote Sensing/Photogrammetry, Switzerland, 119–146

Schwaller MR, Morris KR. 2011 A Ground Validation Network for the Global Precipitation Measurement Mission. J. Atmos. Oceanic Technol 28 : 301–319. DOI: 10.1175/2010JTECHA1403.1

Seto S, and Iguchi T. 2015 Intercomparison of Attenuation Correction Methods for the GPM Dual-Frequency Precipitation Radar. J. Atmos. Oceanic Technol 32 : 915–926. DOI: 10.1175/JTECH-D-14-00065.1

Sims EM, Liu G. 2015 A Parameterization of the Probability of Snow-Rain Transition. J. Hydrometeor. 16 : 1466–1477. DOI: 10.1175/JHM-D-14-0211.1

Shepherd JM, Burian S, Liu C, Bernardes S. 2016 Satellite Precipitation Metrics to Study the Energy-Water-Food Nexus within the Backdrop of an Urbanized Globe. Earthzine. [Available online at http://earthzine.org/2016/05/31/satellite-precipitation-metrics-to-study-the-energywater-food-nexus-within-the-backdrop-of-an-urbanized-globe]

Shi R, Tao WK, Matsui T, Cifelli R, Hou A, Lang S, Tokay A, Wang NY, Peters-Lidard C, Skofronick-Jackson G, Rutledge S, Petersen W. 2010 WRF Simulations of the 20–22 January 2007 Snow Events over Eastern Canada: Comparison with in-situ and Satellite Observations. J. Appl. Meteor. Climatol 49 : 2246–2266. DOI: 10.1175/2010JAMC2282.1

Shige S and Kummerow CD. 2016 Precipitation-Top Heights of Heavy Orographic Rainfall in the Asian Monsoon Region. J. Atmos. Sci 73:8, 3009–3024

Skofronick-Jackson G, Petersen WA, Berg W, Kidd C, Stocker EF, Kirschbaum DB, Kakar R, Braun SA, Huffman GJ, Iguchi T, Kirstetter PE, Kummerow C, Meneghini R, Oki R, Olson WS, Takayabu YN, Kurukawa K, Wilheit T. 2017 The Global Precipitation Measurement (GPM) Mission for Science and Society. Bull. Amer. Meteor. Soc DOI: 10.1175/BAMS-D-15-00306.1

Skofronick-Jackson GM, Johnson BT, Munchak SJ. 2013 Detection Thresholds of Falling Snow from Satellite-Borne Active and Passive Sensors. IEEE Transactions on Geoscience and Remote Sensing. 51 : 4177–4189. DOI: 10.1109/TGRS.2012.2227763

Stanley T, Kirschbaum DB. 2017 A heuristic approach to global landslide susceptibility mapping. Nat. Hazards. 87: 145–164. DOI: 10.1007/s11069-017-2757-y

Stephens GL, Vane DG, Boain RJ, Mace GG, Sassen K, Wang Z, Illingworth AJ, O'Connor EJ, Rossow WB, Durden SL, Miller SD, Austin RT, Benedetti A, Mitrescu C, and CloudSat Science Team. 2002 The CloudSat mission and the A-Train: A new dimension of space-based

NASA Author Manuscript NASA Author Manuscript NASA Author Manuscript

observations of clouds and precipitation. Bull. Amer. Meteorol. Soc 83 : 1771–1790. DOI: 10.1175/BAMS-83-12-1771

Tan BZ, Petersen WA, Tokay A. 2016a A Novel Approach to Identify Sources of Errors in IMERG for GPM Ground Validation. J. Hydrometeor 17 : 121–137. DOI: 10.1175/JHM-D-160079.1

Tan BZ, Petersen WA, Kirstetter P, Tian Y. 2016b Performance of IMERG as a Function of Spatiotemporal Scale. J. Hydrometeor 18 : 307–319. DOI: 10.1175/JHM-D-16-0174.1

Tang G, Wen Y, Gao J, Long D, Ma Y, Wan W, Hong Y. 2017 Similarities and differences between three coexisting spaceborne radars in global rainfall and snowfall estimation. Water Resour. Res, 53 : 3835–3853. DOI: 10.1002/2016WR019961

Tao J Wu D, Gourley J, Zhang SQ, Crow W, Peters-Lidard CD, Barros A 2016 Operational hydrological forecasting during the IPHEx-IOP campaign – Meet the challenge. J. Hydrol 531 : 434–456. DOI: 10.1016/j.jhydrol.2016.02.019

Tao WK, Wu D, Matsui T, Peters-Lidard C, Lang S, Hou A, Reinecker M, Petersen WA. 2013 The diurnal variation of precipitation during MC3E: A modelling study. J. Geophys. Res 118 : 7199–7218. DOI: 10.1002/jgrd.50410/asset/jgrd50410

Tapiador FJ, Navarro A, Levizzani V, García-Ortega E, Huffman GJ, Kidd C, Kucera PA, Kummerow CD, Masunaga H, Petersen WA, Roca R, Sánchez J-L, Tao W-K, Turk FJ, 2017: Global Precipitation Measurements for Validating Climate Models. Atmos. Res, 197, 120. doi:10.1016/j.atmosres.2017.06.021

Thurai M, Gatlin PN, Bringi VN, Petersen W, Kennedy P, Notaros B, Carey LD. 2017 Toward Completing the Raindrop Size Spectrum: Case Studies Involving 2D-Video Disdrometer, Droplet Spectrometer, and Polarimetric Radar Measurements. J. Appl. Meteor. Soc 56 : 877–896. DOI: 10.1175/JAMC-D-16-0304.1

Tian Y, Peters-Lidard C, Harrison K, Prigent C, Norouzi H, Aires F, Boukabara SA, Furuzawa F, Masunaga H. 2013 Quantifying Uncertainties in Land-Surface Microwave Emissivity Retrievals. IEEE Transactions on Geoscience and Remote Sensing. 52 : 829–840. DOI:10.1109/TGRS.2013.2244214

Tiira J, Moisseev DN, von Lerber A, Ori D, Tokay A, Bliven LF, Petersen W. 2016 Ensemble mean density and its connection to other microphysical properties of falling snow as observed in southern Finland. Atmos. Meas. Tech 9 : 4825–4841. DOI: 10.5194/amt-9-4825-2016

Tokay A, D'Adderio L, Porcu F, Wolff D, Petersen W. 2017 A Field Study of Footprint-Scale Variability of Raindrop Size Distribution. J. Hydrometeor 16 : 1855–1868. DOI: 10.1175/JHM-D-15-0159.1

Toyoshima K, Masunaga H, Furuzawa FA. 2015 Early Evaluation of Ku- and Ka-Band Sensitivities for the Global Precipitation Measurement (GPM) Dual-Frequency Precipitation Radar (DPR). SOLA. 11: 14–17. DOI: 10.2141/sola.2015-004

Trenberth K 2011 Changes in precipitation with climate change. Clim. Res 47 : 123–138. DOI: 10.3354/cr00953

Turk FJ, Li L, Haddad ZS. 2014 A Physically Based Soil Moisture and Microwave Emissivity Data Set for Global Precipitation Measurement (GPM) Applications. IEEE Transactions on Geoscience Remote Sensing. 52 : 7637–7650. DOI: 10.1109/TGRS.2014.2315809

Tyynelä J, Chandrasekar V. 2014 Characterizing falling snow using multifrequency dual-polarization measurements. J. Geophys. Res. Atmos 119 : 2169–8996. DOI: 10.1002/2013JD021369

Valle D, Zaitchik B, Feingold B, Spangler K, Pan W. 2013 Abundance of water bodies is critical to guide mosquito larval control interventions and predict risk of mosquito-borne diseases. Parasit. Vectors 6 : 1–2. DOI: 10.1186/1756-3305-6-179 [PubMed: 23281838]

Vega M, Chandrasekar V, Carswell J, Beauchamp RM, Schwaller MR, Nguyen CM. 2014 Salient features of the dual-frequency, dual-polarized, Doppler radar for remote sensing of precipitation. Radio Sci. 49 : 1087–1105. DOI: 10.1002/2014RS005529

Vijayaraj V, Bright EA, Bhaduri BL. 2007 High Resolution Urban Feature Extraction for Global Population Mapping using High Performance Computing. Proceedings of 2007 IEEE International geosciences and remote sensing symposium, IGARSS 2007.

NASA Author Manuscript NASA Author Manuscript NASA Author Manuscript

von Lerber A, Moisseev D, Marks D, Petersen W, Harri A, Chandrasekar V. 2017 Validation of satellite-based snowfall products by using a combination of weather radar and surface observations. J. Appl. Meteorol. and Clim, accepted with minor revision..

Wang J, Adler R, Huffman G, Bolvin D. 2014 An Updated TRMM Composite Climatology of Tropical Rainfall and Its Validation. J. Climate 27 : 273–284. DOI: 10.1175/JCLI-D-13-00331.1

Wen Y, Kirstetter P, Hong Y, Gourley JJ, Cao Q, Zhang J, Flamig Z, Xue X. 2016 Evaluation of a Method to Enhance Real-Time, Ground Radar–Based Rainfall Estimates Using Climatological Profiles of Reflectivity from Space. J. Hydrometeor 17 : 761–775. DOI: 10.1175/JHM-D-150062.1

Wentz FJ, Draper D. 2016 On-Orbit Absolute Calibration of the Global Precipitation Measurement Microwave Imager. J. Atmos. Oceanic Technol 33 : 1393–1412. DOI: 10.1175/JTECH-D-15-0212.1

Wilheit T, Berg W, Ebrahami H, Kroodsma R, McKague D, Payne V, Wang J. 2015 Intercalibrating the GPM constellation using the GPM microwave imager (GMI). Geoscience and Remote Sensing Symposium (IGARSS), 2015 IEEE International DOI: 10.1109/IGARSS.2015.7326996

Williams CR, Bringi VN, Carey LD, Chandrasekar V, Gatlin PN, Haddad ZS, Meneghini R, Munchak SJ, Nesbitt SW, Petersen WA, Tanelli S, Tokay A, Wilson A, Wolff DB. 2014 Describing the shape of raindrop size distributions using uncorrelated raindrop mass spectrum parameters. J. Appl. Meteor. Climatol 53 : 1282–1296. DOI: 10.1175/JAMC-D-13-076.1

Wolff DB, Marks D, Petersen WA. 2014 General application of the Relative Calibration Adjustment (RCA) technique for monitoring and correcting radar reflectivity calibration. J. Atmos. Oceanic Technol 32 : 496–506. DOI: 10.1175/JTECH-D-13-00185.1

Wright DB, Kirschbaum DB, Yatheendradas S. 2017 Satellite Precipitation Characterization, Error Modelling, and Error Correction Using Censored Shifted Gamma Distributions. J. Hydrometeorol DOI:10.1175/JHM-D-17-0060.1

Wu H, Adler RF, Tian Y, Huffman GJ, Li H, Wang J. 2014 Real-time global flood estimation using satellite-based precipitation and a coupled land surface and routing model. Water Resour. Res 50 : 2693–2717. DOI: 10.1002/2013WR014710

You Y, Wang NY, Ferraro R, Rudlosky S. 2016 Quantifying the Snowfall Detection Performance of the Global Precipitation Measurement (GPM) Microwave Imager Channels over Land. J. Hydrometeor 17 : 1101–1117. DOI: 10.1175/JHM-D-16-0190.1

Zagrodnick JP, McMurdie LA, and Houze RA Jr., 2017: Stratiform Precipitation Processes in Cyclones Passing over a Coastal Mountain Range. J. Atmos. Sci, submitted.

Zaitchik BF, Feingold B, Valle D, Pan W. 2014 Integrating Earth Observations to Support Malaria Risk Monitoring in the Amazon. Earthzine. [Available online at http://www.earthzine.org/2014/04/14/integrating-earth-observations-to-support-malaria-riskmonitoring-in-the-amazon/]

Zhang J, Howard K, Langston C, Kaney B, Qi Y, Tang L, Grams H, wang Y, Cocks S, Martinaitis S, Arthur A, Cooper K, Brogden J. 2016 Multi-Radar Multi-Sensor (MRMS) Quantitative Precipitation Estimation: Initial Operating Capabilities. Bull. Amer. Meteor. Soc 97 : 621–638. DOI: 10.1175/BAMS-D-14-00174.1

Zhang SQ, Matsui T, Cheung S, Zupanski M, Peters-Lidard C. 2017 Impact of assimilated precipitation-sensitive radiances on the NU-WRF simulation of West African monsoon. Mon. Wea. Rev DOI: 10.1175/MWR-D-16-0389.1

NASA Author Manuscript

NASA Author Manuscript

NASA Author Manuscript

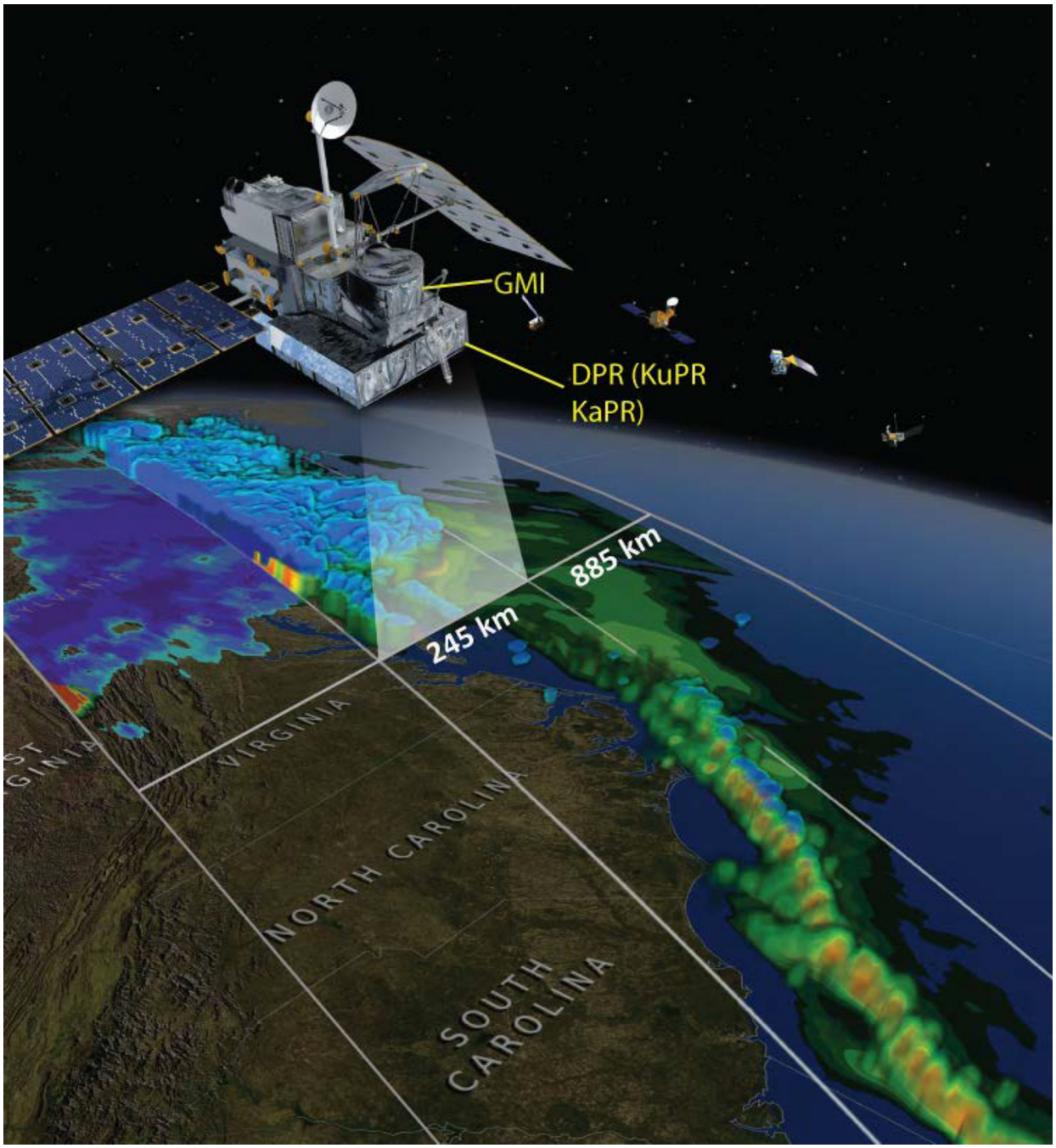

Figure 1:

GPM Core Observatory observations of a snow and rain event off the Carolina coastlines on 17 December 2016. Falling snow is shown in blues to purples, rain is in greens to reds. The GMI has a swath width of 885 km, DPR Ku has a swath of 245 km, while DPR Ka currently has a swath of 125 km (not shown). GMI channels have resolutions of 6–26 km while the DPR resolutions are at 5 km horizontally, and 250 m or 500 m vertically, depending on operating mode (Hou *et al.*, 2014).

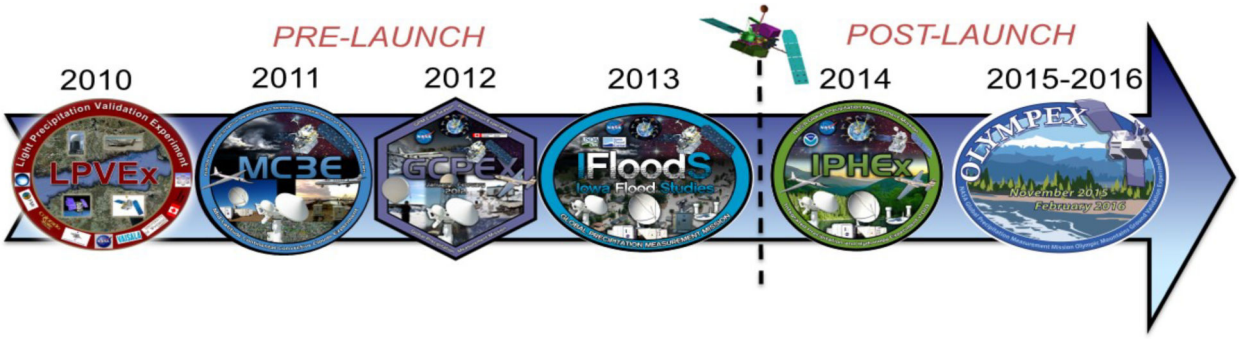

Figure 2:
Timeline of pre- and post-launch field campaigns for the GPM Ground Validation program: 2010 Light Precipitation Validation Experiment (LPVEX), 2011 Mid-latitude Continental Convective Clouds Experiment (MC3E), 2012 GPM Cold Season Precipitation Experiment (GCPEX), 2013 Iowa Floods Studies (IFLOODS), 2014 Integrated Precipitation and Hydrology Experiment (IPHEx), 2015–2016 Olympic Mountains Experiment (OLYMPLEX).

NASA Author Manuscript
NASA Author Manuscript
NASA Author Manuscript

NASA Author Manuscript

NASA Author Manuscript

NASA Author Manuscript

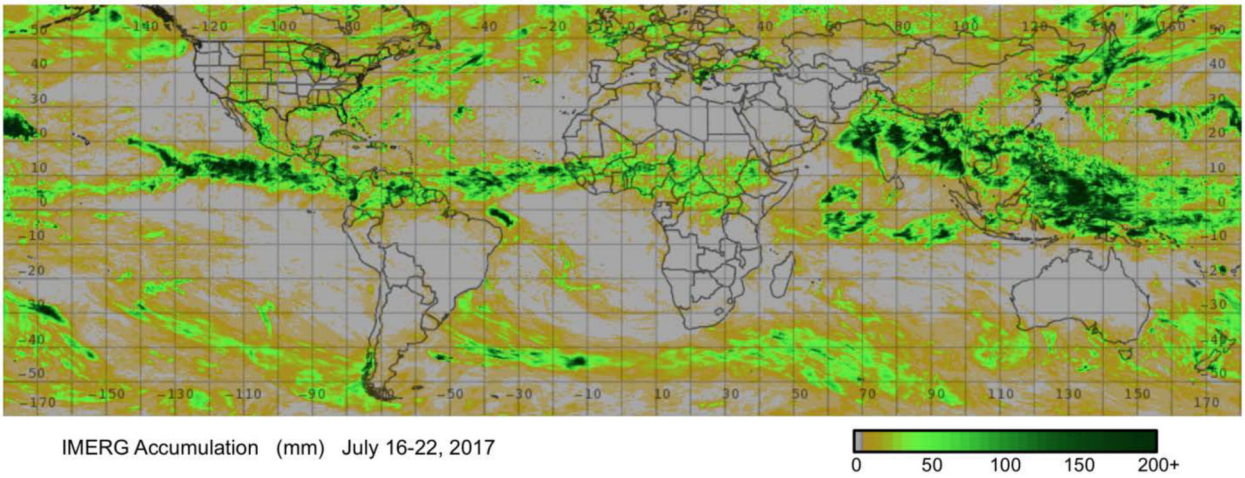

Figure 3:

The nearly global U.S. team's IMERG precipitation dataset provides rainfall rates every thirty minutes. This map of Version 04 Late Run data show rainfall accumulations from 16–22 July 2017.

NASA Author Manuscript NASA Author Manuscript NASA Author Manuscript

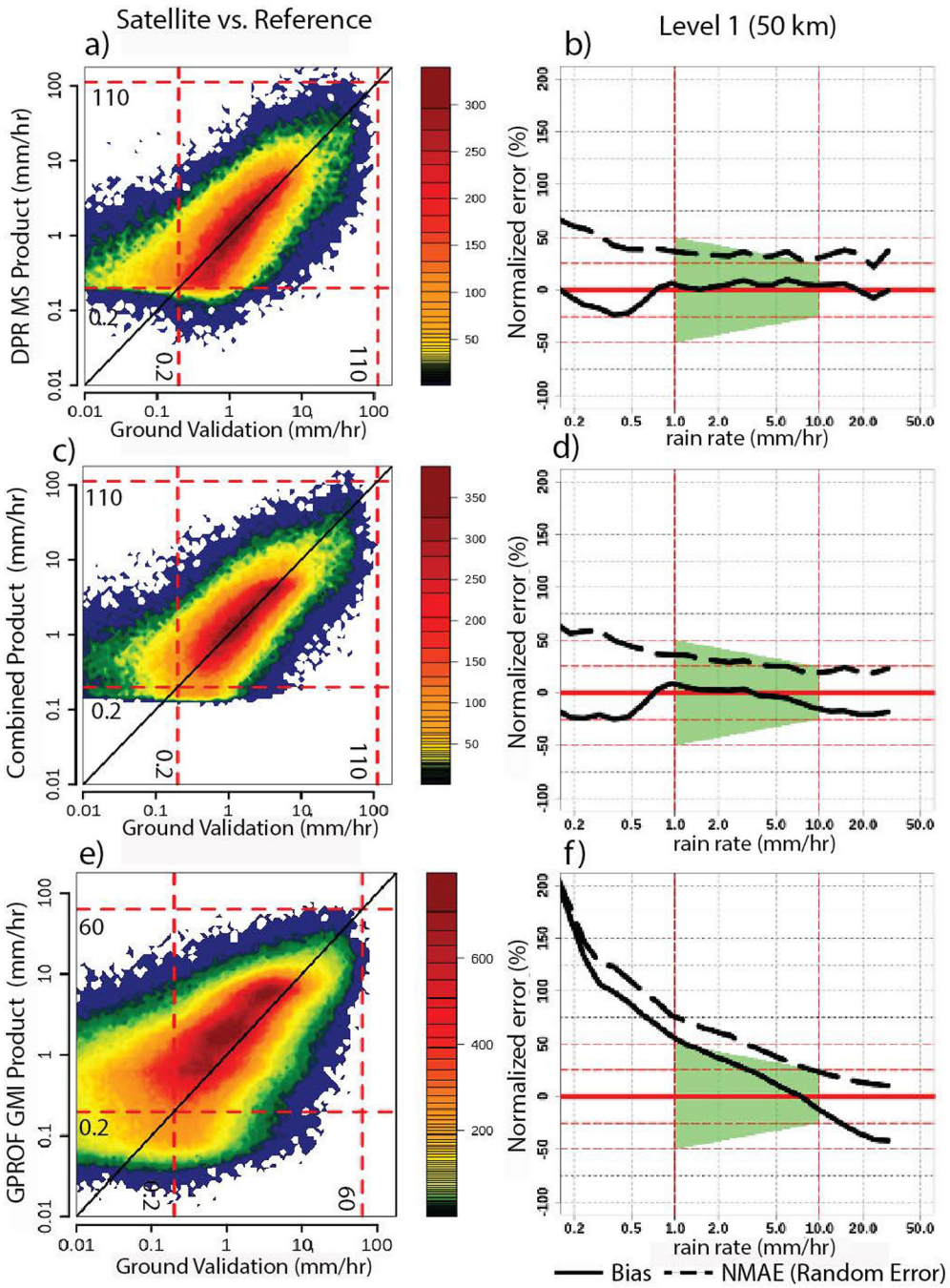

Figure 4:

Validation of DPR (a,b), CORRA (c,d) and GPROF GMI Products (e,f). The left column shows the satellite product verses ground validation reference for instantaneous rain rates at native resolution (5 km footprint for DPR and CORRA and 15 km EVOF for GPROF GMI. Dashed lines in left column indicate that each product meets the requirements of 0.2–110 mm h^{-1} for DPR and 0.2–60 for GMI. The right column shows results averaged over 50 km for bias and normalized mean absolute error (NMAE) random error to be < 25% at 10 mm h

$^{-1}$ and <50% at 1 mm h^{-1} as indicated in the green shaded area. The DPR data are from Version 05 and are the Matched Scan (Ku+Ka) retrievals

NASA Author Manuscript
NASA Author Manuscript
NASA Author Manuscript

NASA Author Manuscript

NASA Author Manuscript

NASA Author Manuscript

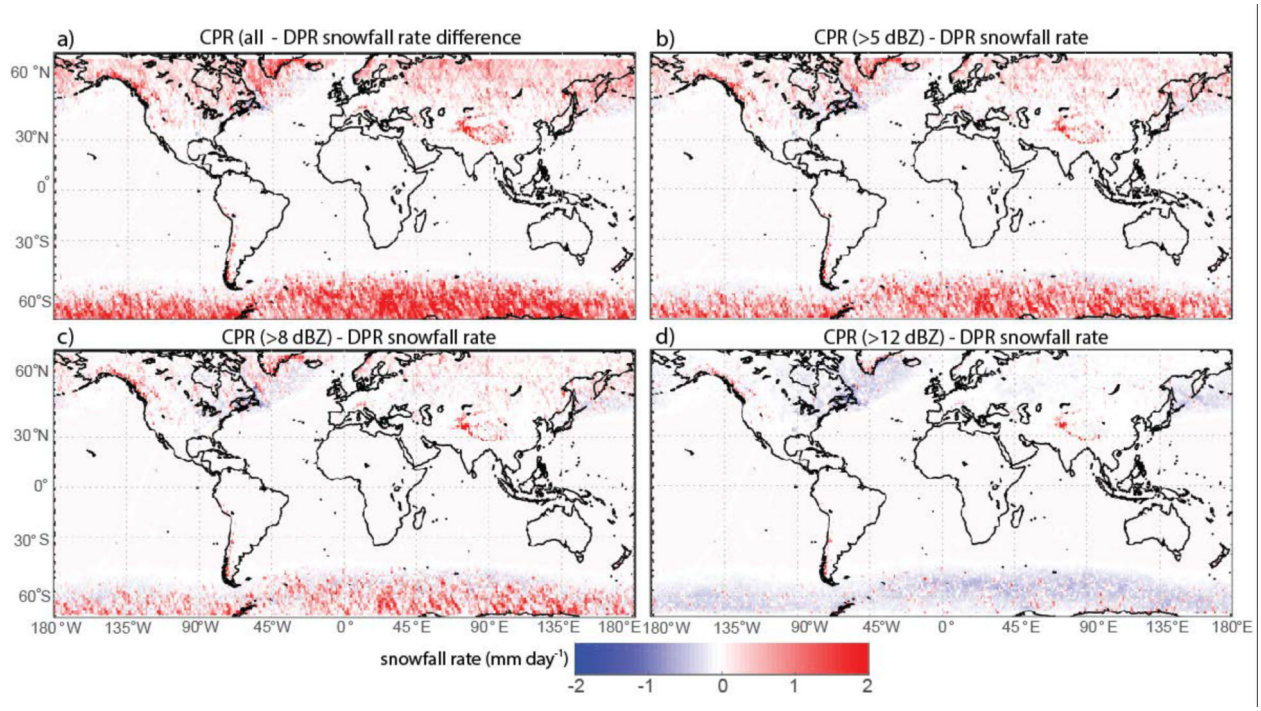

Figure 5:

CloudSat falling snow estimates using several minimum detectable reflectivity thresholds as compared to DPR falling snow retrievals. Falling snow rate differences are in mm day^{-1} and averaged over 1°×1° latitude-longitude grid boxes for the period 03/2014–03/2016 for CloudSat and 03/2014–12/2016 for DPR. Differences are (CloudSat – GPM DPR Normal Scan [NS]) falling snow estimates for CloudSat reflectivities that are a) > −28 dBZ (all CloudSat data), b) >5 dBZ, c) >8 dBZ, and d) >12 dBZ. Note that the official DPR falling snow products have been modified here to report the falling snow at the surface using the Sims and Liu (2015) temperature at 2m rain/snow indicator.

NASA Author Manuscript

NASA Author Manuscript

NASA Author Manuscript

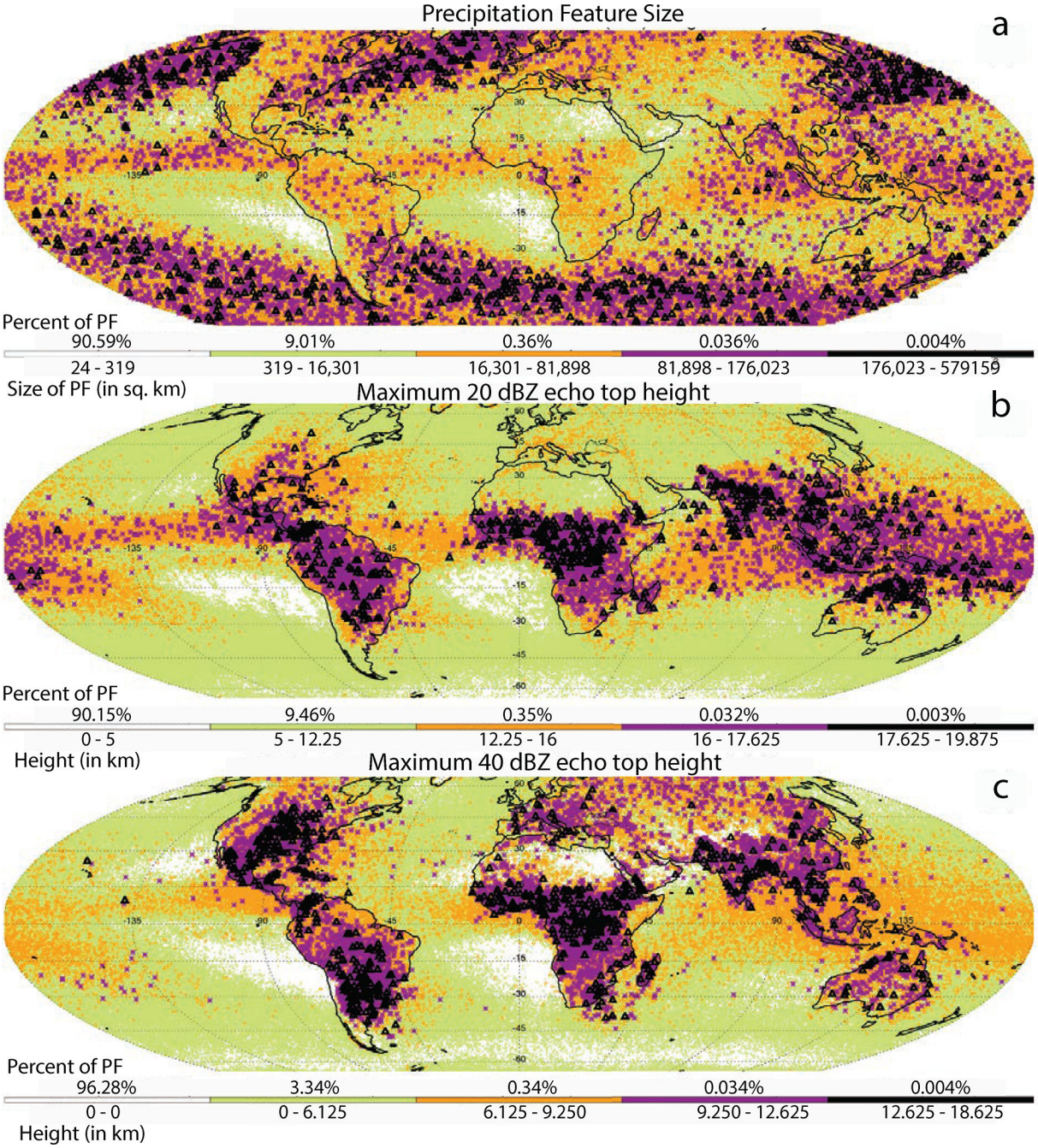

Figure 6:

GPM-CO data from 2014–2017 showing the locations of precipitation features (PF) according to their size, DPR-Ku 20 dBZ, and 40 dBZ maximum echo top height.

NASA Author Manuscript

NASA Author Manuscript

NASA Author Manuscript

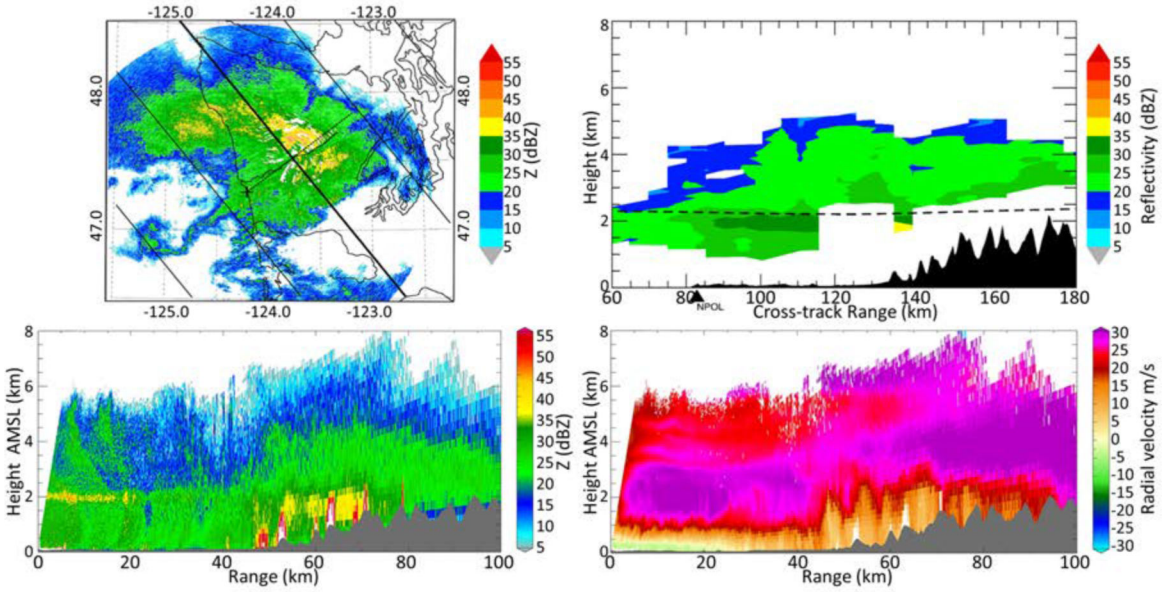

Figure 7:

Precipitation sampled during the GPM OLYMPEX overpass of 1523 UTC, 3 December 2015. a) NPOL 1.5° PPI of effective radar reflectivity factor (Z) with GPM track (bold line) and DPR Ku-band normal and matched scan boundaries indicated (light lines). A dashed line extending northeast of NPOL represents the orientation of cross-sections in panels (b)-(d); b) DPR Ku Normal Scan range-height cross-section of corrected-Z along the dotted line in (a), terrain shaded in black, position of NPOL indicated; c) NPOL range-height scan of Z along the DPR cross-section illustrating orographic enhancements over terrain and below the melting layer in regions of clutter-contaminated DPR data; d) as in (c) but NPOL radial velocity (negative values toward NPOL, positive values away).

NASA Author Manuscript

NASA Author Manuscript

NASA Author Manuscript

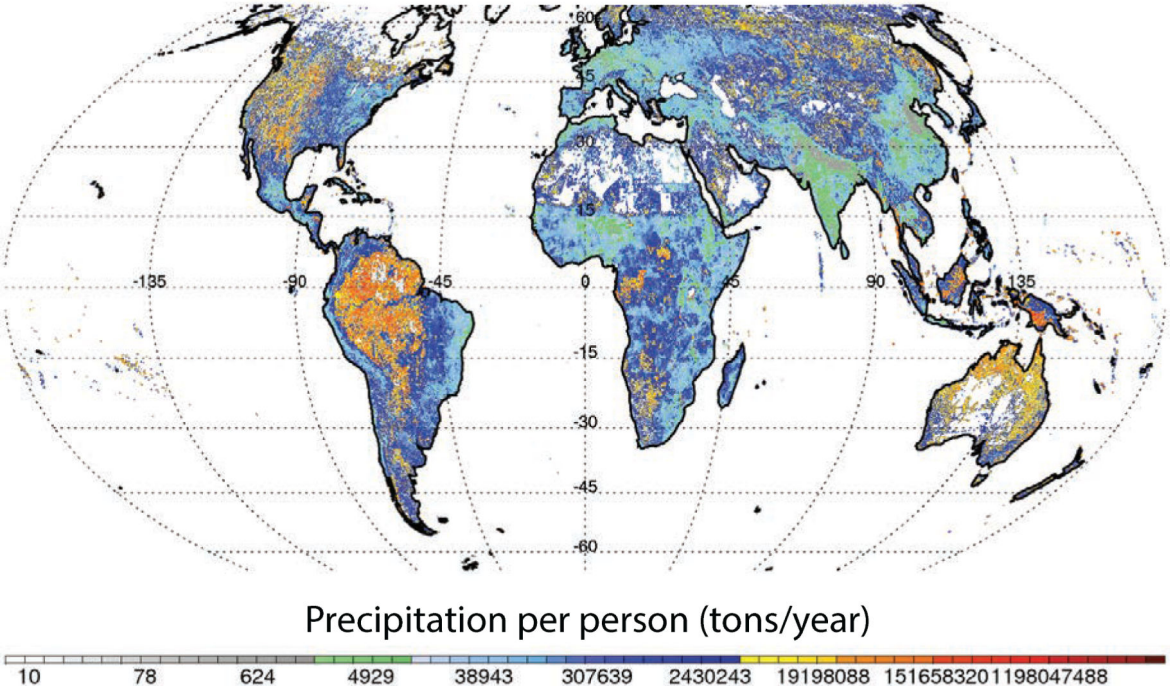

Figure 8:

Mean precipitation per person (PPP) (ton/year) at 0.1˚ resolution (Shepherd *et al.*, 2016), calculated using IMERG precipitation information and population density from LandScan global population dataset (Vijayaraj *et al.*, 2007).

NASA Author Manuscript

NASA Author Manuscript

NASA Author Manuscript

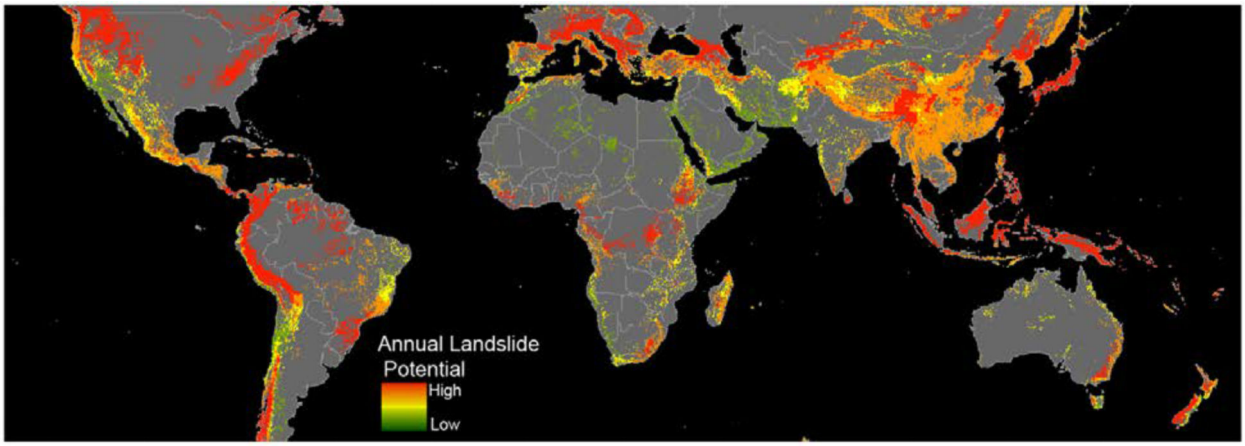

Figure 9:

Distribution of annually averaged landslide nowcasts using a model that brings together TMPA precipitation data and a global susceptibility map (Stanley and Kirschbaum, 2017).

NASA Author Manuscript

NASA Author Manuscript

NASA Author Manuscript

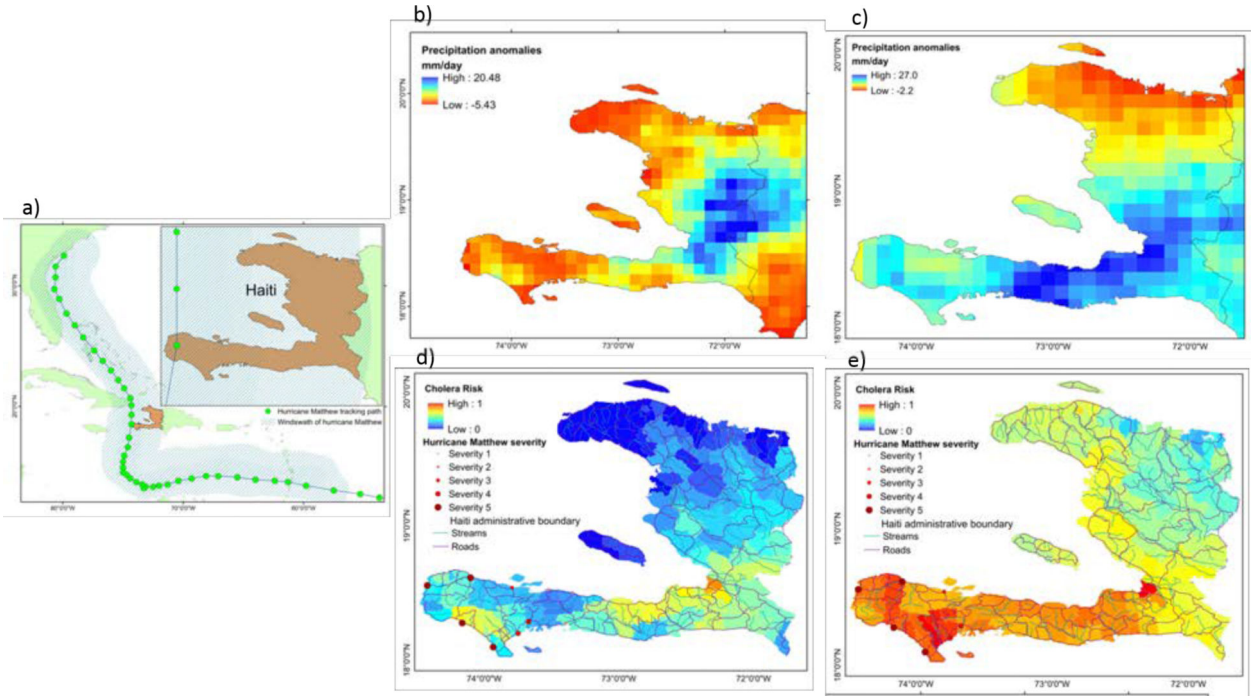

Figure 10:

GPM IMERG data enabled estimates of cholera risk following the passage of Hurricane Matthew across Haiti on 1–2 October 2016. Plots show a) Hurricane Matthew's track, highlighting the study area in Haiti, b) September 2016 IMERG precipitation anomalies, c) 14 September-13 October 2016 precipitation anomalies, d) Cholera risk map based on pre-hurricane hydro-climatic conditions, and e) Cholera risk map based on 2 weeks post hurricane hydroclimatic conditions. Figure modified from Khan *et al.* (2017).

NASA Author Manuscript

NASA Author Manuscript

NASA Author Manuscript

Table I.

GPM constellation members, including the satellite, sensor, scanning mode, type of instrument, launch date and mission end. These include the passive microwave imagers (MWI), TRMM Microwave Imager (TMI), Special Sensor Microwave Image Sounder (SSMIS), GPM Microwave Imager (GMI), Advanced Microwave Scanning Radiometer-2 (AMSR2); the passive microwave sounders (MWS), Microwave Humidity Sounder (MHS), Advanced Technology Microwave Sounder (ATMS); and the radar or active microwave (AMW), Precipitation Radar (PR) and Dual-frequency Precipitation Radar (DPR). The spacecraft include NASA-JAXA GPM and TRMM satellites, the U.S. NOAA series, the U.S. Defense Meteorological Satellite Program (DMSP) series, the European Union Meteorological Satellites: MetOp-A and Metop-B, the French-Indian Megha-Tropiques satellite, the U.S. NPOESS Preparatory Project (NPP) satellite, and the Japanese Global Change Observation Mission 1st - Water (GCOM-W1) satellite. References are provided in Hou *et al.* (2014).

Satellite	Sensor	Scanning	Type	Launch	Until
TRMM	TMI	Conical	MWI	1997-11-27	2015-04-08
	PR	Cross-track	AMW		
DMSP F16	SSMIS	Conical	MWI	2003-10-18	
NOAA18	MHS	Cross-track	MWS	2005-05-20	
MetOpA	MHS	Cross-track	MWS	2006-10-19	
DMSP F17	SSMIS	Cross-track	MWI	2006-11-05	
NOAA19	MHS	Cross-track	MWS	2009-02-06	
DMSP F18	SSMIS	Conical	MWS	2009-10-18	
Megha-Tropiques	SAPHIR	Cross-track	MWS	2011-10-12	
NPP	ATMS	Cross-track	MWS	2011-10-28	
GCOM-W1	AMSR2	Conical	MWI	2012-05-17	
MetOpB	MHS	Cross-track	MWS	2012-09-17	
GPM-CO	GMI	Conical	MWI	2014-02-27	
	DPR	Cross-track	AMW		
DMSP F19	SSMIS	Conical	MWI	2014-04-03	2016-02-11

NASA Author Manuscript

NASA Author Manuscript

NASA Author Manuscript

Table II.

Summary description of GPM data products by the Product Level (1–4). Version 05 of the Level 2 algorithms became available for download in May 2017. National products are those designed and implemented by NASA or JAXA independently. Standard products require joint approval from a governing board composed of both NASA and JAXA representatives.

Product Level	Description	Coverage
Level 1B GMI	Geolocated and inter-calibrated brightness temperatures; Standard product	Swath, Instantaneous Field of View (IFOV)
Level 1B DPR	Geolocated and calibrated radar powers; JAXA National product	Swath, IFOV
Level 1C, GMI and partner radiometers, Note GMI 1B=GMI 1C	Inter-calibrated brightness temperatures; NASA National product	Swath, IFOV
Level 2 GMI (GPROF algorithm)	Radar enhanced precipitation retrievals; Standard product	Swath, IFOV
Level 2 partner radiometers (GPROF algorithm)	Radar enhanced precipitation retrievals from 1C; NASA National Product	Swath, IFOV
Level 2 DPR (DPR algorithm)	Reflectivities, sigma zero, characterization, PSD, precipitation with vertical structure; Standard product	Swath, IFOV (Normal Scan (NS) for Ku, High Sensitivity (HS) for Ka, and Matched Scan (MS) for Ku+Ka)
Level 2 combined GMI+DPR (CORRA algorithm)	Precipitation; Standard product	Swath, IFOV (initially at DPR Ku swath and then at GMI swath)
Level 3 Latent Heating (GMI, DPR, CORRA)	Latent heating and associated related parameters; Standard product	0.25° x 0.25° monthly grid
Level 3 Instrument Accumulations	GMI, partner radiometers, CORRA and DPR; Standard product	0.25° x 0.25° monthly grid
Level 3 Merged Products	Merger of GMI, partner radiometer, and IR; IMERG: NASA National product GSMaP: JAXA National product	As fine as: IMERG: 0.1° x 0.1° 30minute grid GSMaP: 0.1° x 0.1° 60minute grid
Level 4 Products	Model-assimilated precipitation forecast and analysis: NASA National product	Model temporal and spatial scales (planned)

NASA Author Manuscript

NASA Author Manuscript

NASA Author Manuscript

Table III.

GPM product latency requirements and average latency statistics for the first three years of operation. NRT, research, and climate products, use varying levels of ancillary data.

Product	End-to-End (to user) Latency Requirement (90% of the time)	Percentage of Time Met (avg. to 25 Jan 2017)	Average Latency Statistics (averaged over # months, # files)
GMI L1 Tb	NRT: 1 hour	99.9	17.4 minutes (5mo, 29,581 files)
GMI GPROF L2 Precipitation	NRT: 1 hour	98.8	23.2 min (8 mo., 59,442 files)
	Research product: No requirement	N/A	Approximately 24 hours
	Climate Product: No requirement	N/A	Approximately 3 months
DPR L2 Precipitation	No requirement	N/A	76.2 min (20 mo., 20,053 files)
	Research product: No requirement	N/A	Approximately 24 hours
DPR+GMI CORRA L2 Precipitation	NRT: 3 hours	98.0	83.5 min (20 mo., 26,239 files)
	Research product: No requirement	N/A	Approximately 24 hours
L3 IMERG	No requirement	N/A	Early Run: approximately 4 hrs, goal 3 hrs
			Late Run: approximately 12 hrs
			Late Run: approximately 3 months

NASA Author Manuscript

NASA Author Manuscript

NASA Author Manuscript

Table IV.

Primary GPM Ground Validation field campaigns. Note that this table does not include several GPM international partner-led campaigns that hosted smaller complements of NASA GPM instrumentation in Brazil, Canada, France, Italy, and South Korea. In the Instruments column, field campaigns use airborne remote sensing (R) and *in situ* microphysical (M), as well as ground-based instrumentation.

Campaign	Instruments	Description	Data Access
LPVEX 2010	R, M, radar, gauge disdrometer, ADMIRARI* radiometer, rawinsonde	*Light Precipitation Validation Experiment.* High-latitude cold, light rain over ocean and continental land surfaces. Joint with CloudSat GV.	https://ghrc.nsstc.nasa.gov/home/field-campaigns/lpvex
MC3E 2011	R, M, radar, gauge disdrometer, ADMIRARI radiometer rawinsonde	*Mid-latitude Continental Convective Clouds Experiment.* Warm-season mid-latitude convective and stratiform precipitation. Joint with the Department of Energy-Atmospheric Radiation Measurement facility. (Jensen *et al.*, 2016)	https://ghrc.nsstc.nasa.gov/home/field-campaigns/mc3e https://www.arm.gov/data
GCPEX 2012	R, M, radar, gauge disdrometer, ADMIRARI radiometer, rawinsonde	*GPM Cold Season Precipitation Experiment.* Mid-latitude snow in synoptic and lake-effect environments. Joint with Environment Canada. (Skofronick-Jackson *et al.*, 2016)	https://ghrc.nsstc.nasa.gov/home/field-campaigns/ https://ghrc.nsstc.nasa.gov/home/field-campaigns/gcpex
IFloodS 2013	Radar, gauge, disdrometer, soil moisture, streamflow	*Iowa Floods Studies.* Warmseason mid-latitude mesoscale precipitation events and integrated hydrologic validation. Joint with Iowa Flood Center.	https://ghrc.nsstc.nasa.gov/home/field-campaigns/ifloods
IPHEx 2014	R, M, radar, gauge, disdrometer, rawinsonde	*Integrated Precipitation and Hydrology Experiment.* Warmseason orographic precipitation and integrated hydrologic validation (Barros *et al.*, 2014)	https://ghrc.nsstc.nasa.gov/home/field-campaigns/iphex http://iphex.pratt.duke.edu/
OLYMPEX 2015/16	R, M, radar, gauge, disdrometer, rawinsonde, dropsonde, snow camera	*Olympic Mountains Experiment.* Cold-season orographic and oceanic rainfall and snow; integrated hydrologic validation. Joint with NASA Radar Experiment (RADEX). (Houze *et al.*, 2017)	https://ghrc.nsstc.nasa.gov/home/field-campaigns/olympex http://olympex.atmos.washington.edu/

* ADMIRARI = Advanced Microwave Radiometer Rain Identification

NASA Author Manuscript

NASA Author Manuscript

NASA Author Manuscript

Table V.

List of TRMM and GPM societal benefit areas, topics, and specific uses of the data.

Societal Benefit Area	Topic	Application
Extreme Events and Disasters	Flooding	Incorporation in hydrologic routing models for flood estimation
	Landslides	Nowcasting of potential landslide activity, rainfall intensity and duration characteristics for landslide occurrence
	Tropical Cyclones	Improved characterization of tropical cyclone track and intensity
	Wildfires	Management and situational awareness of rainfall accumulation in affected areas
	Disaster Response Re-insurance and Insurance	Situational awareness of extreme precipitation in potentially affected areas Definition of extreme precipitation thresholds to determine payouts for Microinsurance or improve situational awareness for precipitation climatologies
Water Resources & Agriculture	Drought	Evaluation of precipitation anomalies leveraging extended temporal record
	Water Resource Management	Assessment of freshwater input to basins and reservoirs to better quantify water fluxes
	Agricultural Applications and Food Security	Integration of precipitation data within agricultural models to estimate growing season onset, crop productivity and other variables
Weather and Climate Modelling	Numerical Weather Prediction	Assimilation of Level 1 brightness temperatures within NWP modelling for initializing model runs
	Land Surface Modelling	Data assimilation into land surface models to estimate environmental variables
	Climate Variability and Change	Verification and validation of seasonal and climate modelling
Public Health & Ecology	Disease Tracking	Tracking precipitation anomalies with environmental conditions for disease vectors or water-borne diseases
	Ecological Forecasting	Monitor changes in precipitation that are associated with migration patterns
Technology and Policy	Satellite services and Data Distribution	Supporting data distribution, ground systems services